Title

Mechanosensory Genes Pkd1 and Pkd2 Contribute to the Planar Polarization of Brain Ventricular Epithelium.

Journal

Journal of Neuroscience, 35(31)

Authors

Ohata, Shinya
Herranz-Pérez, Vicente
Nakatani, Jin
et al.

Publication Date

2015-08-05

DOI

10.1523/JNEUROSCI.0686-15.2015

Peer reviewed

Development/Plasticity/Repair

Mechanosensory Genes *Pkd1* and *Pkd2* Contribute to the Planar Polarization of Brain Ventricular Epithelium

Shinya Ohata (大畑慎也),[1] Vicente Herranz-Pérez,[2,3] Jin Nakatani (中谷仁),[4] Alessandra Boletta,[5] José Manuel García-Verdugo,[2,3] and Arturo Álvarez-Buylla[1]

[1]Department of Neurological Surgery, and Eli and Edythe Broad Center of Regeneration Medicine and Stem Cell Research, University of California, San Francisco (UCSF), San Francisco, California 94143, [2]Laboratorio de Neurobiología Comparada, Instituto Cavanilles, Universidad de Valencia, CIBERNED, 46980 Valencia, Spain, [3]Unidad Mixta de Esclerosis Múltiple y Neurorregeneración, IIS Hospital La Fe, 46026 Valencia, Spain, [4]Biomedical MR Science Division, Shiga University of Medical Science, Ohtsu, Shiga 520-2192, Japan, and [5]Division of Genetics and Cell Biology, San Raffaele Scientific Institute, 20132 Milan, Italy

Directional beating of ependymal (E) cells' cilia in the walls of the ventricles in the brain is essential for proper CSF flow. E cells display two forms of planar cell polarity (PCP): rotational polarity of individual cilium and translational polarity (asymmetric positioning of cilia in the apical area). The orientation of individual E cells varies according to their location in the ventricular wall (location-specific PCP). It has been hypothesized that hydrodynamic forces on the apical surface of radial glia cells (RGCs), the embryonic precursors of E cells, could guide location-specific PCP in the ventricular epithelium. However, the detection mechanisms for these hydrodynamic forces have not been identified. Here, we show that the mechanosensory proteins polycystic kidney disease 1 (Pkd1) and Pkd2 are present in primary cilia of RGCs. Ablation of *Pkd1* or *Pkd2* in *Nestin-Cre;Pkd1*$^{flox/flox}$ or *Nestin-Cre;Pkd2*$^{flox/flox}$ mice, affected PCP development in RGCs and E cells. Early shear forces on the ventricular epithelium may activate Pkd1 and Pkd2 in primary cilia of RGCs to properly polarize RGCs and E cells. Consistently, Pkd1, Pkd2, or primary cilia on RGCs were required for the proper asymmetric localization of the PCP protein Vangl2 in E cells' apical area. Analyses of single- and double-heterozygous mutants for *Pkd1* and/or *Vangl2* suggest that these genes function in the same pathway to establish E cells' PCP. We conclude that Pkd1 and Pkd2 mechanosensory proteins contribute to the development of brain PCP and prevention of hydrocephalus.

Key words: cilia; ependymal cell; epithelium; neural stem cell; planar cell polarity; polycystin

Significance Statement

This study identifies key molecules in the development of planar cell polarity (PCP) in the brain and prevention of hydrocephalus. Multiciliated ependymal (E) cells within the brain ventricular epithelium generate CSF flow through ciliary beating. E cells display location-specific PCP in the orientation and asymmetric positioning of their cilia. Defects in this PCP can result in hydrocephalus. Hydrodynamic forces on radial glial cells (RGCs), the embryonic progenitors of E cells, have been suggested to guide PCP. We show that the mechanosensory proteins Pkd1 and Pkd2 localize to primary cilia in RGCs, and their ablation disrupts the development of PCP in E cells. Early shear forces on RGCs may activate Pkd1 and Pkd2 in RGCs' primary cilia to properly orient E cells. This study identifies key molecules in the development of brain PCP and prevention of hydrocephalus.

Introduction

Ependymal (E) cells are multiciliated epithelial cells that line the brain ventricles and generate CSF flow through ciliary beating (Miyan et al., 2003). E cells exhibit two types of planar cell polarity (PCP): (1) rotational polarity, the unidirectional orientation of individual basal bodies (BBs), and (2) translational polarity, the asymmetric positioning of the cluster of BBs in the apical

Received Feb. 19, 2015; revised June 25, 2015; accepted July 8, 2015.

Author contributions: S.O. and A.Á.-B. designed research; S.O., V.H.-P., J.N., A.B., and J.M.G.-V. performed research; S.O., V.H.-P., A.B., J.M.G.-V., and A.Á.-B. analyzed data; S.O. and A.Á.-B. wrote the paper.

This work was sponsored by grants from the National Institutes of Health (NIH, HD032116 and NS028478) and a generous gift from the J. G. Bowes Foundation; S.O. was supported by the Cell Science Research Foundation, the Kanae Foundation for the Promotion of Medical Science, TOYOBO Biotechnology Foundation, and the Japanese Society for Promotion of Science; A.Á.-B. holds the Heather and Melanie Muss Endowed Chair. We thank Drs. L. S. Goldstein, A. Messing, G. Schütz, T. Watnick, and B. K. Yoder for providing mice; T. Inubushi, A. Kriegstein, P. McQuillen, and M. Ramalho-Santos for sharing equipment; A. Cebrián-Silla, Y.-G. Han, Z. Mirzadeh, M. F. Paredes, I. Rowe, L. Subramanian, and C. K. Tong for technical advice; L. Bogdanova, M. Castelli, J. L. Elsbernd, S. González-Granero, C. Guinto, J. R. Rodriguez, R. Romero, and A. Rudik for technical help; J. L. Elsbernd and M. F. Paredes for proofreading; and the A.Á.-B. laboratory for useful discussion.

The authors declare no competing financial interests.

Correspondence should be addressed to either of the following: Dr Shinya Ohata, Graduate School of Pharmaceutical Sciences, University of Tokyo, 7-3-1 Hongo, Bunkyo, Tokyo 113-0033, Japan, E-mail: ohata@mol.f.u-tokyo.ac.jp; or Dr Arturo Álvarez-Buylla, Department of Neurological Surgery, University of California, San Francisco, San Francisco, CA 94143, E-mail: ABuylla@stemcell.ucsf.edu.

DOI:10.1523/JNEUROSCI.0686-15.2015

 0270-6474/15/3511153-16$15.00/0

region of E cells toward the direction of CSF flow (Mirzadeh et al., 2010b). Defects in E cells' PCP result in abnormal CSF accumulation and hydrocephalus (Boutin et al., 2014; Ohata et al., 2014; Ying et al., 2014). Understanding the mechanism underlying the establishment of E cell PCP is important for the diagnosis and prevention of hydrocephalus.

Translational polarity begins in the embryonic progenitors of E cells, called radial glial cells (RGCs), by the embryonic day (E)16 (Mirzadeh et al., 2010b; Boutin et al., 2014). The early asymmetric localization of BB in RGCs is further refined as they differentiate into E cells (Mirzadeh et al., 2010b). Rotational polarity of individual motile cilia, which in immature E cells is random, becomes unidirectional during E cells' maturation between postnatal day (P)4 and P20 (Guirao et al., 2010). Both rotational and translational polarity are well correlated with the direction of CSF flow (location-specific PCP; Mirzadeh et al., 2010b; Boutin et al., 2014), suggesting that the early passive CSF flow could influence the development of PCP in RGCs and E cells. Hydrodynamic forces can instruct rotational polarity in cultured developing E cells and multiciliated cells in the *Xenopus* larval skin (Mitchell et al., 2007; Guirao et al., 2010). Interestingly, RGCs' primary cilia, which protrude into the ventricles, are required for the proper polarization of E cells (Mirzadeh et al., 2010b). The primary cilium is emerging as a key sensory organelle with many functions, including mechanosensation (Guemez-Gamboa et al., 2014). Early hydrodynamic forces on the ventricular surface of RGCs has been proposed to help guide the planar polarization of E cells (Mirzadeh et al., 2010b). The molecular components involved in the establishment of PCP in RGCs and E cells remain unknown.

The mechanosensory protein polycystic kidney disease 1 (Pkd1; also known as polycystin-1 and PC-1) is an 11-pass transmembrane protein, enriched in primary cilia, and has been proposed to mediate mechanosensation of urine flow in the kidney (Nauli et al., 2003; Zhou, 2009; Kotsis et al., 2013). Activation of Pkd1 by fluid flow triggers Ca^{2+} intake through its associated ion channel, Pkd2 (also known as polycystin-2, PC-2, and transient receptor potential polycystic 2; Nauli et al., 2003). Genetic inactivation of *Pkd1* affects convergent extension-like movement and oriented cell division in kidney epithelial cells (Luyten et al., 2010; Castelli et al., 2013), suggesting its involvement in PCP. Interestingly, ablation of *Pkd1* in the developing mouse brain results in hydrocephalus (Wodarczyk et al., 2009). However, whether Pkd1 or Pkd2 play a role in the E cells' planar polarization, and how these mechanoreceptor components help organize the ventricular epithelium remains unknown.

Here, we show that Pkd1 and Pkd2 are expressed in primary cilia of RGCs. Ablation of *Pkd1* or *Pkd2* in early RGCs using *Nestin-Cre;Pkd1*$^{flox/flox}$ or *Nestin-Cre;Pkd2*$^{flox/flox}$ mutant mice did not affect the differentiation of E cells, but significantly disrupted PCP in both RGCs and E cells. The core PCP protein van Gogh-like 2 (Vangl2) is asymmetrically localized in RGCs' and E cells' apical compartment, and it is required for their PCP (Guirao et al., 2010; Boutin et al., 2014). Interestingly, in the *Nestin-Cre;Pkd1*$^{flox/flox}$, *Nestin-Cre;Pkd2*$^{flox/flox}$ or ciliary mutants (*Nestin-Cre;Kif3a*$^{flox/flox}$ and *Nestin-Cre;Ift88*$^{flox/flox}$), the asymmetric localization of Vangl2 in the apical region of E cells was severely disrupted. Double-heterozygous mutants for *Pkd1* and *Vangl2* resulted in synergistic phenotypes, suggesting that these genes function in the same pathway for E cells' PCP. These results identify Pkd1 and Pkd2 as key mechanosensory components in RGCs to establish PCP in the ventricular epithelium of the postnatal brain.

Materials and Methods

Animals. All animal experiments were approved by the Institutional Animal Care and Use Committee and Laboratory Animal Resource Center at UCSF, and maintained following the NIH, American Veterinary Medical Association, and UCSF guidelines. *hGFAP-Cre* (Zhuo et al., 2001), *Ift88*^{flox} (Haycraft et al., 2007), *Kif3a*^{flox} (Marszalek et al., 2000), *Nestin-Cre* (Tronche et al., 1999), *Pkd1*^{flox} (Wodarczyk et al., 2009), and *Pkd2*^{flox} (Garcia-Gonzalez et al., 2010; The Jackson Laboratory, 017292) mice have been previously generated and were genotyped as described. *Vangl2*^{Lp} mice (The Jackson Laboratory, 000220) were identified previously (Strong and Hollander, 1949; Kibar et al., 2001; Murdoch et al., 2001) and were genotyped by PCR using the following primers (*Lp* WT F, 5′-CAA ACA GTG GAC CTT GGT GTG-3′; *Lp* mutant F, 5′-CAA ACA GTG GAC CTT GGT GTA-3′; *Lp* WT and mutant R, 5′-TGG CAG AAA TGT GTC AGG G-3′). Both males and females were used for all experiments.

Reverse transcription-PCR. cDNAs were generated from microdissected lateral walls of the lateral ventricles at P0 as described previously (Ohata et al., 2009, 2011). The following primers were used; *Pkd1* F, 5′-GGA CTA TGA GAT GGT GGA GC-3′; *Pkd1* R, 5′-GAG AGG AAG GAG GTC CAT TG-3′; *Pkd2* F, 5′-TCA AGC TGG AGA TCA TGG AG-3′; Pkd2 R, 5′-CTC AGG AAC ACA CAA ACA CG-3′; *ef1αF, 5′-GCT TTG AGT GAA GCT CTT CC-3′; ef1αR, 5′-CCT TCT TGT CCA CAG CTT TG-3′*.

Immunohistochemistry. Mice were deeply anesthetized with 700 mg/kg bodyweight tribromoethanol (Sigma-Aldrich) by intraperitoneal injections. For the preparation of cryosections, brains were dissected after transcardial perfusion with saline (0.9% NaCl) and 4% paraformaldehyde (PFA, Sigma-Aldrich) in 100 mM phosphate buffer (PB), pH 7.4, using a 323E pump (Watson Marlow, 3–4 ml/min), postfixed with 4% PFA at 4°C overnight, rinsed with PBS, incubated in 30% sucrose overnight, immersed in OCT compound (Sakura) at 4°C for 1 h, frozen on dry ice in OCT compound, and sectioned at 12 μm thickness with a HM 500 OM cryostat (Microm). The cryosections were washed with PB at 4°C for 15 min, and permeabilized with 0.1% Triton X-100 (Sigma-Aldrich) in PBS at room temperature (20–22°C) for 15 min. Antigen retrieval was performed in 10 mM citrate buffer, pH 6.0, at 95°C for 10 min. Next, blocking of nonspecific binding sites was performed with PBS with 10% normal donkey serum (Sigma-Aldrich) and 0.5% Triton X-100 (blocking solution). Primary antibodies were incubated in the blocking solution overnight at 4°C followed by secondary antibody and 4′,6-diamidino-2-phenylindole (DAPI; Sigma-Aldrich) incubation at room temperature for 2 h.

Whole-mounts of the lateral ventricle walls were prepared as described previously (Mirzadeh et al., 2010a). The exposed walls were fixed in 4% PFA at 4°C overnight and washed with PBS/0.2% Triton X-100 three times. For Pkd2 staining, antigen retrieval was performed in 10 mM citrate buffer, pH 6.0, at 95°C for 10 min. After blocking, whole-mounts were incubated with primary antibodies in the blocking solution overnight at 4°C, washed with PBS/0.2% Triton X-100, and incubated with secondary antibodies in the blocking solution overnight at 4°C.

Confocal images were taken on a Leica SP5 using a HCX PL APO CS 100× oil-immersion objective lens (NA 1.46). To analyze BB patch angle in E cells and BB angle in RGCs, the vectors were drawn using MetaMorph software as described previously (Mirzadeh et al., 2010b). The angles of the vectors were normalized so that the average of the angle of the vectors is 180° in each picture. The percentages of vectors were plotted on a histogram in 15° bins. BB patch displacement in E cells and BB displacement in RGCs were quantified using the ImageJ software (NIH). To normalize the magnitude of the vector for the size and shape of the apical surface in each E cell, we divided it by the length of line that is drawn from the center of the apical surface to the edge of the apical surface passing through the center of BB patch (see Fig. 7*a*, black line). The intensity of Vangl2-immunoreactivity in the apical area of E cells was quantified using the MetaMorph software and normalized to control mice.

Antibodies. Primary antibodies: rabbit anti-adenylyl cyclase type III (ACIII, Santa Cruz Biotechnology, sc-588), mouse anti-β-catenin (BD

Biosciences, 610153), rabbit anti-β-catenin (Sigma-Aldrich, C2206), rat anti-CD24-conjugated with phycoerythrin (PE; BD Biosciences, 553262), mouse anti-FoxJ1 (eBiosciences, 14-9965), chicken anti-GFAP (aves, GFAP), mouse anti-HA (Covance Research Products, MMS-101P-200), rabbit isotype control (Cell Signaling Technology, no. 3900), rabbit anti-Pkd1 (Bioss, bs-2157R), rabbit anti-Pkd2 (EMD Millipore, AB9088), rabbit anti-S100β (Dako, Z0311), mouse anti-acetylated tubulin (Sigma-Aldrich, T6793), rabbit anti-γ-tubulin (Sigma-Aldrich, T5192), rabbit anti-Vangl2 (Santa Cruz Biotechnology, sc-67136). Secondary antibodies: conjugated to AlexaFluor dyes (donkey or goat polyclonal, Thermo Fisher Scientific).

Scanning electron microscopy. Whole-mount preparations of the lateral wall of lateral ventricles were fixed with 2% PFA and 2.5% glutaraldehyde (Electron Microscopy Sciences; EMS) in PB at room-temperature for 1 h, washed with PB, postfixed with 1% osmium tetroxide (EMS) in PB for 2 h at room temperature, rinsed with deionized water, and dehydrated first in ethanol then with CO_2 by critical point drying method. The samples were coated with gold/palladium alloy by sputter coating. The surface of the lateral wall was studied under a Hitachi S-4800 scanning electron microscope using Quantax 400 software (Bruker) for image acquisition.

Transmission electron microscopy. Whole-mount preparations of the lateral wall of lateral ventricles were fixed overnight with 2% PFA and 2.5% glutaraldehyde (EMS) in PB at 4°C, washed with PB, postfixed with 2% osmium tetroxide (EMS) in PB for 2 h at room temperature, rinsed with PB, stained with 2% uranyl acetate (EMS) in 70% ethanol at 4°C for 2.5 h, dehydrated with ethanol, incubated in propylene oxide (EMS), and embedded in Durcupan resin (Sigma-Aldrich). Serial semithin sections (1.5 μm) were cut with an UC-6 ultramicrotome (Leica) and stained lightly with 1% toluidine blue. Subsequently, selected levels were glued with Super Glue-3 Loctite (Henkel) to Araldite blocks and detached from the glass slide by repeated freezing in liquid nitrogen and thawing. Ultrathin sections (60–70 nm) were prepared with an ultramicrotome and stained with lead citrate (Reynolds' solution). Photomicrographs were obtained under a FEI Tecnai G^2 Spirit transmission electron microscope (FEI Europe) using a Morada digital camera (Olympus Soft Image Solutions). Acquired images were analyzed using ImageJ software.

Image processing. Adjustment of brightness and contrast of the pictures, if required, was performed using Photoshop CS5 (Adobe Systems) or ImageJ software.

High-speed live imaging of ciliary beating and ependymal flow assay. Whole-mounts of the lateral wall of the lateral ventricle were freshly dissected as above. For high-speed imaging of ciliary beating, the whole-mount preparations were incubated with rat anti-CD24 antibody conjugated with PE in neurobasal medium (Thermo Fisher Scientific) supplemented with B-27 serum-free supplement (Thermo Fisher Scientific), glutamine and antibiotics for 20 min at room temperature, rinsed with L-15 medium (Thermo Fisher Scientific), and placed in a glass bottomed dish (BD Biosciences). Low melting point agarose (1–2%; Thermo Fisher Scientific) and Neurobasal medium with the supplements were placed on the whole-mounts. Ciliary beating was recorded with 15 ms exposure time at 61 frames per second (fps) for 200 frames at room temperature using a Leica DMI600 B microscope, HCX PL APO 100× oil-immersion objective lens (NA 1.44, Leica), Rolera EM-C^2 high-speed camera (QImaging), and MetaMorph software.

For the ependymal flow assay, a glass micropipette filled with fluorescent polystyrene latex microbeads (2 μm, Polysciences) attached to an MO-10 micromanipulator (Narishige) was lowered onto the whole-mount and microbeads were deposited onto the ventricular surface. The movement of microbeads was recorded using a Leica MZFLIII fluorescent dissection microscope and Retiga 2000R high-speed digital camera (QImaging) plugged into OpenLab imaging software (Improvision) at 10 fps. The speeds of migrating fluorescent beads were quantified using the Manual Tracking plugin for ImageJ software.

Magnetic resonance imaging. T2-weighted axial image sequences of fixed brains were acquired using a 7T MR scanner (Unity Inova system; Agilent Technologies) and a handmade proton surface coil (repetition time/echo time = 4200/36 ms, 10 × 10 mm, thickness = 0.5 mm, slice gap = 0 mm). Obtained images were analyzed using ImageJ software.

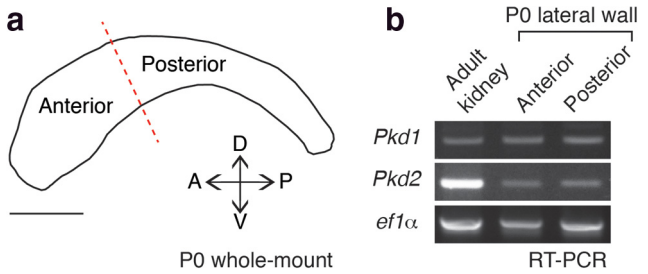

Figure 1. *Pkd1* and *Pkd2* were expressed in microdissected lateral walls of the lateral ventricle. ***a***, Schematic drawing of the lateral wall of the lateral ventricle at P0. The red dotted line indicates the border between the anterior and posterior regions used for RT-PCR analysis. A, Anterior; D, dorsal; P, posterior; V, ventral. Scale bar, 1 mm. ***b***, RT-PCR showing that *Pkd1* and *Pkd2* are expressed both in the anterior and posterior regions of lateral walls of the lateral ventricle at P0. *ef1α* was used as a loading control.

Statistics. All results shown in the dot plot graphs are expressed as mean ± SEM. The means of experimental groups were compared with two-tailed Student's *t* test. The distributions of angles were compared with Watson's U^2 test using Oriana software (Kovach Computing Services). Distribution of the Vangl2 asymmetric localization positive and negative cells between control and mutant mice was compared with Fisher's exact test using Prism 6 software (Graphpad). Differences were considered significant at $p < 0.05$.

Results

Localization of Pkd1 and Pkd2 in primary cilia of RGCs

We first investigated, using reverse transcription-PCR (RT-PCR), whether *Pkd1* and *Pkd2* were expressed in lateral walls of the lateral ventricle at P0 (Fig. 1*a*). Both mRNAs were present in microdissected ventricular wall (Fig. 1*b*). To determine the subcellular localization of Pkd1 in RGCs, we used a knock-in mouse line that expresses influenza hemagglutinin (HA)-tagged Pkd1 (hereafter referred to as $Pkd1^{flox/flox}$, also known as $Pkd1^{HA/HA}$; Wodarczyk et al., 2009). Immunolabeling for Pkd1-HA revealed staining associated with the shaft of P0 RGCs' primary cilia (Fig. 2*a*, arrows), with some punctate staining outside the cilia in the apical domain (Fig. 2*a*, arrowheads). This staining was not observed in wild-type (WT) controls (Fig. 2*b*). To confirm the specificity of the HA-immunostaining, we crossed the $Pkd1^{flox/flox}$ mice with *Nestin-Cre* transgenic mice (hereafter referred to as *Nestin-Cre;*$Pkd1^{flox/flox}$) to eliminate Pkd1 C terminus domain, including the HA-tag, in the developing brain beginning at E9.5 (Tronche et al., 1999). In these mice, no Pkd1-HA staining was observed in cilia (Fig. 2*c*), demonstrating the specificity of Pkd1-HA immunoreactivity. Immunostaining using an antibody against Pkd1 also showed punctate staining associated with primary cilia and in the apical region of RGCs (Fig. 2d, arrows and arrowheads, respectively). Pkd2 was also detected in primary cilia of P0 RGCs in WT and $Pkd2^{flox/flox}$ mice, but not in *Nestin-Cre;* $Pkd2^{flox/flox}$ mice (Fig. 2*e–g*). Immunoreactivity was not detected in RGCs stained with isotype control antibody (Fig. 2*h*), further suggesting the specificity of the antibody against Pkd1 (Fig. 2*d*) or Pkd2 (Fig. 2*e–g*). In the primary cilia of P0 $Pkd1^{flox/flox}$ RGCs, Pkd1-HA and Pkd2 colocalized (Fig. 3*a–d*). Interestingly, Pkd2 immunolabeling was significantly reduced in primary cilia of RGCs in *Nestin-Cre;*$Pkd1^{flox/flox}$ mice (Fig. 3*e–h*), suggesting that Pkd2 requires Pkd1 to be present in primary cilia of RGCs. These results are consistent with previous reports showing that Pkd1 and Pkd2 physically associate to each other (Qian et al., 1997; Tsiokas et al., 1997; Hanaoka et al., 2000) and that the ciliary localization of Pkd2 depends on the presence of Pkd1 (Nauli et al., 2003; Zhou, 2009; Kim et al., 2014). Adenylyl cyclase type III

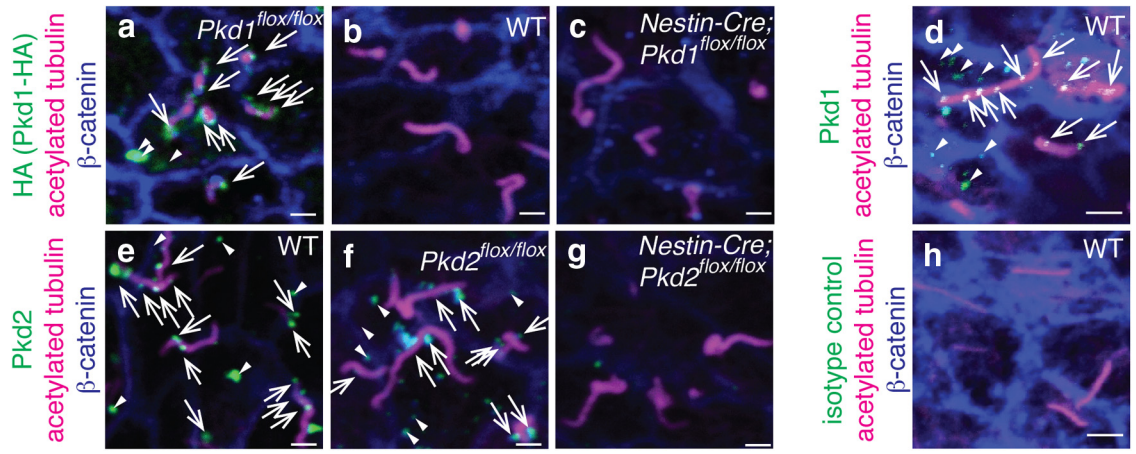

Figure 2. Pkd1 and Pkd2 localized to RGCs' primary cilia. Whole-mount preparations of the lateral walls of lateral ventricle from Pkd1$^{flox/flox}$ (***a***), WT (***b***, ***d***, ***e***, ***h***), Nestin-Cre;Pkd1$^{flox/flox}$ (***c***), Pkd2$^{flox/flox}$ (***f***), and Nestin-Cre;Pkd2$^{flox/flox}$ (***g***) at P0 were stained with antibodies against HA (***a–c***, green, marking Pkd1-HA), Pkd1 (green in d), Pkd2 (***e–g***, green), acetylated tubulin (***a–h***, magenta, marking the primary cilia of RGCs), β-catenin (***a–h***, blue, marking the intercellular junctions between RGCs), or isotype control antibody (***h***, green). White arrows and arrowheads indicate the Pkd1-HA (***a***), Pkd1 (***d***), and Pkd2 (***e***, ***f***) immunoreactivities inside and outside of cilia, respectively. Scale bars: ***a–c***, ***e–g***, 1.0 μm; ***d***, ***h***, 2.5 μm.

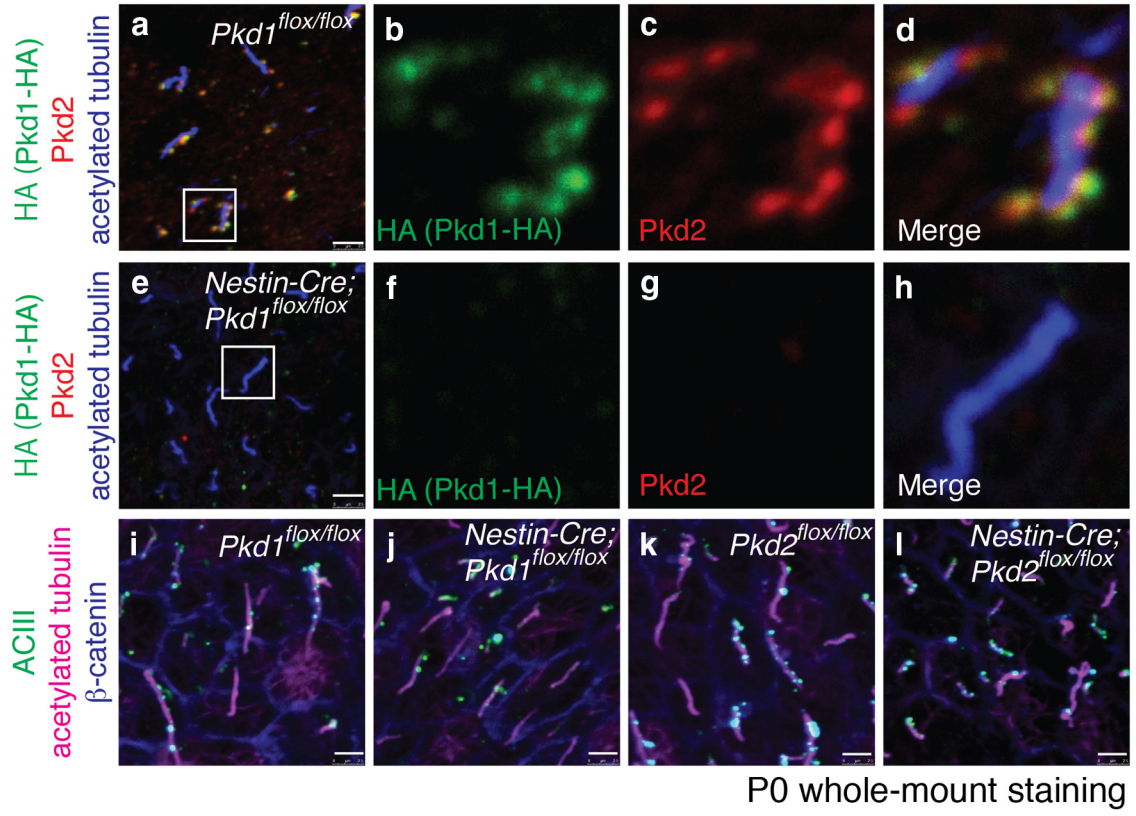

Figure 3. Pkd1 and Pkd2 colocalized in RGCs' primary cilia. Whole-mount preparations of the lateral walls of lateral ventricle from *Pkd1*$^{flox/flox}$ (***a–d***, ***i***), *Nestin-Cre;Pkd1*$^{flox/flox}$ (***e–h***, ***j***), *Pkd2*$^{flox/flox}$ (***k***), and *Nestin-Cre;Pkd2*$^{flox/flox}$ (***l***) at P0 were stained with antibodies against HA (***a***, ***b***, ***d–f***, ***h***, green), Pkd2 (***a***, ***c–e***, ***g***, ***h***, red), acetylated tubulin (***a***, ***d***, ***e***, ***h***, blue; ***i–l***, magenta), ACIII (***i–l***, green), and β-catenin (***i–l***, blue). The insets in ***a*** and ***e*** are magnified in ***b–d*** and ***f–h***, respectively, and shown in separate channels (Pkd1-HA in ***b***, ***f***, green; Pkd2 in ***c***, ***g***, red) and merged images (***d***, ***h***). Yellow signals in ***d*** indicate colocalization of Pkd1-HA and Pkd2. Scale bar, 2.5 μm.

(ACIII) localizes to the primary cilia of RGCs (Higginbotham et al., 2013; Tong et al., 2014). Ciliary localization of ACIII was not affected in P0 RGCs in *Nestin-Cre;Pkd1*$^{flox/flox}$ or *Nestin-Cre;Pkd2*$^{flox/flox}$ mice (Fig. 3*i–l*), demonstrating the specificity of ciliary localization defects in the *Nestin-Cre;Pkd1*$^{flox/flox}$ and *Nestin-Cre;Pkd2*$^{flox/flox}$ RGCs. Altogether, our data indicate that Pkd1 and Pkd2 are present in the developing brain ventricular epithelium and are localized to the primary cilia of RGCs.

Normal differentiation of E cells in *Nestin-Cre;Pkd1*$^{flox/flox}$ and *Nestin-Cre;Pkd2*$^{flox/flox}$ mice

To address the roles of *Pkd1* and *Pkd2* in E cells, we used the *Nestin-Cre;Pkd1*$^{flox/flox}$ and *Nestin-Cre;Pkd2*$^{flox/flox}$ mice. E cells are derived from *Nestin-Cre*-expressing RGCs (Spassky et al., 2005), allowing us to test the role of these genes in the development of E cells. *Nestin-Cre;Pkd1*$^{flox/flox}$ or *Nestin-Cre;Pkd2*$^{flox/flox}$ mice did not display major developmental defect, but by

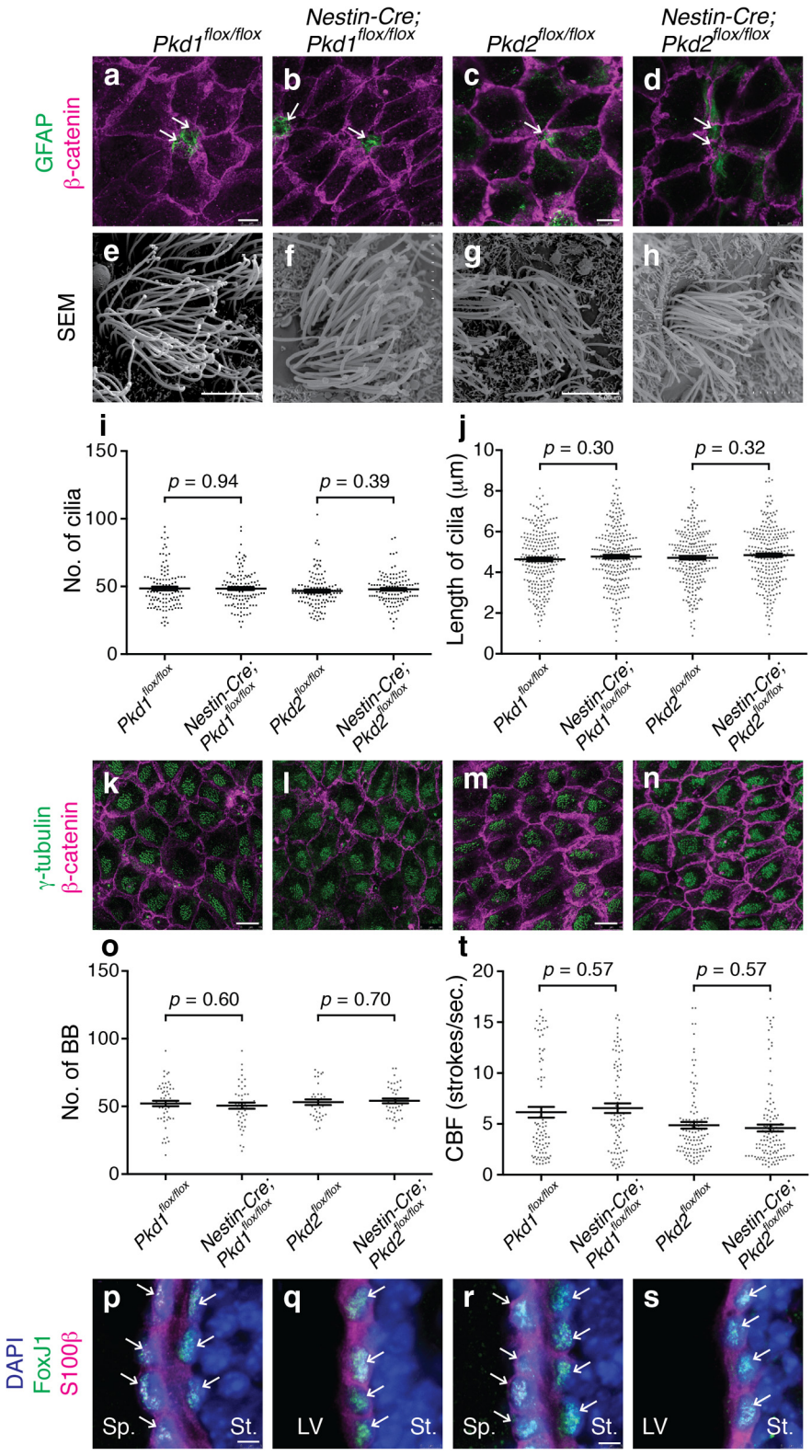

Figure 4. Differentiation of E cells was largely normal in *Nestin-Cre;Pkd1*$^{flox/flox}$ and *Nestin-Cre;Pkd2*$^{flox/flox}$ mice. ***a–d***, The pinwheel organization of E cells surrounding B1 cells' apical endings was preserved in *Nestin-Cre;Pkd1*$^{flox/flox}$ and *Nestin-Cre;Pkd2*$^{flox/flox}$ mice at P21. Whole-mount preparations of the lateral walls of lateral ventricle were stained with antibodies against GFAP (green; apical endings of B1 cells) and β-catenin (magenta, cell borders) in *Pkd1*$^{flox/flox}$ (***a***), *Nestin-Cre;Pkd1*$^{flox/flox}$ (***b***), *Pkd2*$^{flox/flox}$ (***c***), and *Nestin-Cre;Pkd2*$^{flox/flox}$ (***d***) mice at P21. White arrows indicate B1 cells at the center of pinwheel structures. Scale bar, 7.5 μm. ***e–j***, Multiciliation of E cells was normal in *Nestin-Cre;Pkd1*$^{flox/flox}$ and *Nestin-Cre;Pkd2*$^{flox/flox}$ mice at P21. ***e–h***, Whole-mount preparations of the lateral walls of the lateral ventricle were observed by scanning electron microscopy in *Pkd1*$^{flox/flox}$ (***e***), *Nestin-Cre;Pkd1*$^{flox/flox}$ (***f***), *Pkd2*$^{flox/flox}$ (***g***), and *Nestin-Cre;Pkd2*$^{flox/flox}$ (***h***) mice. Scale bar, 5 μm. ***i***, ***j***, The number (***i***) and length (***j***) of E cells' motile cilia were quantified and plotted. Data shown are mean ± SEM. Each point on the graph is the number of an individual E cell (***i***) and the length of an individual cilium (***j***). ***i***, 118 cells from four *Pkd1*$^{flox/flox}$ mice, 121 cells from four *Nestin-Cre;Pkd1*$^{flox/flox}$ mice, $p = 0.94$; 121 cells from four *Pkd2*$^{flox/flox}$ mice, 122 cells from four *Nestin-Cre;Pkd2*$^{flox/flox}$ mice, $p = 0.39$. ***j***, 243 cilia from four *Pkd1*$^{flox/flox}$ mice, 248 cilia from four *Nestin-Cre;Pkd1*$^{flox/flox}$ mice, $p = 0.30$; 244 cilia from four *Pkd2*$^{flox/flox}$ mice, 247 cilia from four *Nestin-Cre;Pkd2*$^{flox/flox}$ mice; $p = 0.32$. ***k–n***, Whole-mount preparations of the lateral walls of the lateral ventricle at P21 were stained with antibodies against γ-tubulin (green) and β-catenin (magenta) in *Pkd1*$^{flox/flox}$ (***k***), *Nestin-Cre;Pkd1*$^{flox/flox}$ (***l***), *Pkd2*$^{flox/flox}$ (***m***), and *Nestin-Cre;Pkd2*$^{flox/flox}$ (***n***) mice. Scale bars, 10 μm. ***o***, The number of BBs was similar in the *Pkd1*$^{flox/flox}$ ($n = 56$ cells from three mice), *Nestin-Cre;Pkd1*$^{flox/flox}$ ($n = 48$ cells from three mice; $p = 0.60$), *Pkd2*$^{flox/flox}$ ($n = 35$ cells from three mice), and *Nestin-Cre;Pkd2*$^{flox/flox}$ ($n = 42$ cells from three mice, $p = 0.70$) E cells. Data shown are mean ± SEM. Each point on the graph is the number of BBs in an individual E cell. ***p–s***, Coronal cryosections were stained with anti-FoxJ1 (green) and anti-S100β (magenta) antibodies and DAPI (blue) in *Pkd1*$^{flox/flox}$ (***p***), *Nestin-Cre;Pkd1*$^{flox/flox}$ (***q***), *Pkd2*$^{flox/flox}$ (***r***), and *Nestin-Cre;Pkd2*$^{flox/flox}$ (***s***) mice. Scale bar, 5 μm. White arrows indicate FoxJ1 and S100β double-positive cells. LV, Lateral ventricle; Sp, septum; St, striatum. Note that two layers of ependyma from the lateral (striatum side) and medial (septum side) walls of the lateral ventricles are shown in controls (***p***, ***r***), whereas only one layer from the lateral wall is shown in *Nestin-Cre;Pkd1*$^{flox/flox}$ (***q***) and *Nestin-Cre;Pkd2*$^{flox/flox}$ (***s***) due to the expansion of the LV in these mutants. ***t***, CBF was unaffected in *Nestin-Cre;Pkd1*$^{flox/flox}$ and *Nestin-Cre;Pkd2*$^{flox/flox}$ mice at P21. Data shown are mean ± SEM. Each point on the graph is CBF of an individual E cell. 86 cells from three *Pkd1*$^{flox/flox}$ mice, 83 cells from three *Nestin-Cre;Pkd1*$^{flox/flox}$ mice, $p = 0.57$; 112 cells from four *Pkd2*$^{flox/flox}$ mice, 120 cells from four *Nestin-Cre;Pkd2*$^{flox/flox}$ mice, $p = 0.57$ (Movies 1–4).

P21 their body size was smaller than that of control littermates (*Pkd1*$^{flox/flox}$ and *Pkd2*$^{flox/flox}$ with no Cre, respectively; *Pkd1*$^{flox/flox}$, 11.1 ± 0.3 g; mean ± SEM; $n = 22$; *Nestin-Cre;Pkd1*$^{flox/flox}$, 8.3 ± 0.3 g, $n = 18$, $p = 0.0001$; *Pkd2*$^{flox/flox}$, 9.8 ± 0.5 g, $n = 9$; *Nestin-Cre;Pkd2*$^{flox/flox}$, 7.0 ± 0.6 g, $n = 9$, $p = 0.0012$), possibly due to polycystic kidney disease (Shillingford et al., 2010). *Nestin-Cre;Pkd1*$^{flox/flox}$ mice also develop hydrocephalus (Wodarczyk et al., 2009), suggesting defects in the developing ventricular system. It remains unknown whether the development or function of E cells is disrupted in *Nestin-Cre;Pkd1*$^{flox/flox}$ mice. The walls of the lateral ventricle contain, in addition to E cells, the small apical surfaces of B1 cells (the ventricular-subventricular zone adult neural stem cells; Fuentealba et al., 2012). E and B1 cells form rosette-like structures known as pinwheels (Mirzadeh et al., 2008). The pinwheel organization, as revealed in whole-mount staining for glial fibrillary acidic protein (GFAP; localized in B1 cells' apical endfoot) and β-catenin (localized to intercellular junctions), was normal in *Nestin-Cre;Pkd1*$^{flox/flox}$

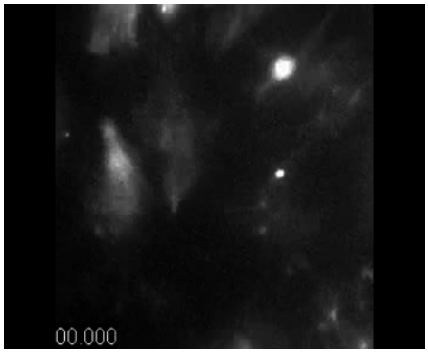

Movies 1. Live imaging movie showing ciliary beating of E cells in *Pkd1*$^{flox/flox}$ mouse.

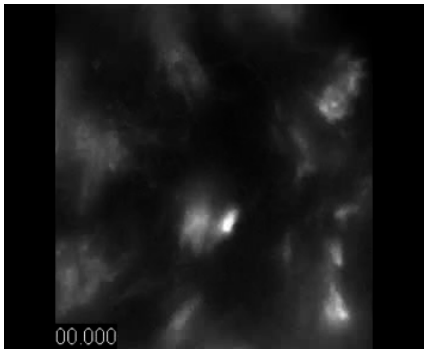

Movies 2. Live imaging movie showing ciliary beating of E cells in *Nestin-Cre;Pkd1*$^{flox/flox}$ mouse.

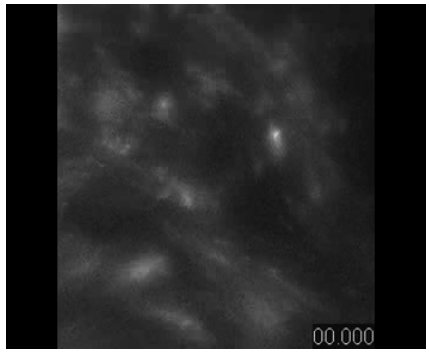

Movies 3. Live imaging movie showing ciliary beating of E cells in *Pkd2*$^{flox/flox}$ mouse.

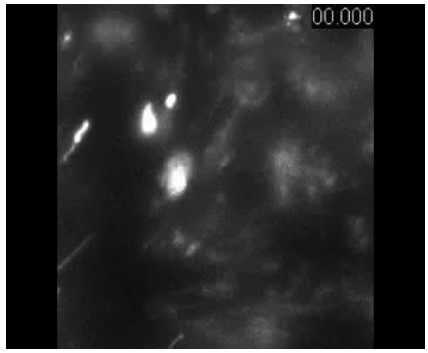

Movies 4. Live imaging movie showing ciliary beating of E cells in *Nestin-Cre;Pkd2*$^{flox/flox}$ mouse.

and *Nestin-Cre;Pkd2*$^{flox/flox}$ mice at P21 (Fig. 4*a–d*). Observation of P21 whole-mounts using scanning electron microscopy revealed that the morphology, number, and length of motile cilia in E cells were similar in *Nestin-Cre;Pkd1*$^{flox/flox}$, *Nestin-Cre;Pkd2*$^{flox/flox}$, and control mice (Fig. 4*e–j*). Whole-mount staining for γ-tubulin, a protein which localizes to BBs, showed that the number of BBs in the apical region of E cells at P21 was unaffected in *Nestin-Cre;Pkd1*$^{flox/flox}$ and *Nestin-Cre;Pkd2*$^{flox/flox}$ compared with control mice (Fig. 4*k–o*). These results suggest that the generation and the apical docking of the BBs (Guirao et al., 2010; Al Jord et al., 2014) was unaffected in *Nestin-Cre;Pkd1*$^{flox/flox}$ and *Nestin-Cre;Pkd2*$^{flox/flox}$ mice. The forkhead transcription factor FoxJ1 and calcium binding protein S100β, which label E cells (Ohata et al., 2014), were normally expressed in E cells in *Nestin-Cre;Pkd1*$^{flox/flox}$ and *Nestin-Cre;Pkd2*$^{flox/flox}$ mice at P21 (Fig. 4*p–s*, arrows). Beating of E cell motile cilia can be visualized using PE-labeled CD24 antibodies (Ohata et al., 2014). We quantified ciliary beating frequency (CBF; strokes/s) in E cells from *Nestin-Cre;Pkd1*$^{flox/flox}$, *Nestin-Cre;Pkd2*$^{flox/flox}$ and control mice at P21. CBF was not affected by deletion of *Pkd1* or *Pkd2* in these mutant mice (Fig. 4*t*; Movies 1–4). These results indicate that E cells differentiate, develop motile cilia, and become organized into pinwheels in *Nestin-Cre;Pkd1*$^{flox/flox}$ and *Nestin-Cre;Pkd2*$^{flox/flox}$ mice.

Requirement of primary cilia, *Pkd1*, and *Pkd2* in the asymmetric localization of Vangl2 in the apical region of E cells

The core PCP protein Vangl2 is a four-pass transmembrane protein that is asymmetrically localized to the apical region of epithelial cells (Montcouquiol et al., 2006; Tissir et al., 2010; Peng and Axelrod, 2012). This protein is required for establishing PCP in various cell types, including E cells (Guirao et al., 2010; Boutin et al., 2014). Primary cilia in RGCs are required for proper establishment of PCP in E cells (Mirzadeh et al., 2010b). To determine whether primary cilia are required for the asymmetric distribution of Vangl2, we used 3 mouse lines: *Nestin-Cre;Kif3a*$^{flox/flox}$, *Nestin-Cre;Ift88*$^{flox/flox}$ and *hGFAP-Cre;Kif3a*$^{flox/flox}$. *Kif3a* and *Ift88* are essential for ciliogenesis (Marszalek et al., 2000; Haycraft et al., 2007). In *Nestin-Cre;Kif3a*$^{flox/flox}$ mice, primary cilia in RGCs are eliminated by E14.5 (Tong et al., 2014) and consequently, E cells never develop motile cilia (Mirzadeh et al., 2010b). In contrast, in *hGFAP-Cre;Kif3a*$^{flox/flox}$ mice Cre-expression is delayed, preserving RGCs primary cilia until around P2, but eliminating E cells' motile cilia (Mirzadeh et al., 2010b). Interestingly, severe PCP defects are observed in the *Nestin-Cre;Kif3a*$^{flox/flox}$ E cells but not in the *hGFAP-Cre;Kif3a*$^{flox/flox}$ E cells (Mirzadeh et al., 2010b), suggesting that the primary cilia in RGCs play a key role in the planar polarization of E cells. The asymmetric localization of Vangl2 on the apical surface of E cells at P21 was conserved in *hGFAP-Cre;Kif3a*$^{flox/flox}$ mice (Fig. 5*a*,*b*; *Kif3a*$^{flox/flox}$, E cells with asymmetric localization of Vangl2/total E cells examined = 76/83, 89%, 4 mice; *hGFAP-Cre;Kif3a*$^{flox/flox}$, 76/92, 84%, 4 mice, $p = 0.21$) as previously demonstrated (Guirao et al., 2010), but it was randomized in *Nestin-Cre;Kif3a*$^{flox/flox}$ and *Nestin-Cre;Ift88*$^{flox/flox}$ mice (Fig. 5*c–f*; *Kif3a*$^{flox/flox}$, 69/119, 58%, 3 mice; *Nestin-Cre;Kif3a*$^{flox/flox}$, 10/83, 12%, 3 mice, $p < 0.0001$; *Ift88*$^{flox/flox}$, 162/243, 67%, 4 mice; *Nestin-Cre;Ift88*$^{flox/flox}$, 10/103, 10%, 4 mice, $p < 0.0001$). This defect in the asymmetric localization of Vangl2 is not due to the long-term expression of Cre in RGCs and E cells, because Vangl2 localization was similar in E cells from *Kif3a*$^{flox/+}$ mice and *Nestin-Cre;Kif3a*$^{flox/+}$ mice (Fig. 5*g*,*h*; *Kif3a*$^{flox/+}$, 114/146, 78%, 4 mice; *Nestin-Cre;Kif3a*$^{flox/+}$, 147/181, 81%, 4 mice; $p = 0.49$). These results indicate that primary cilia in

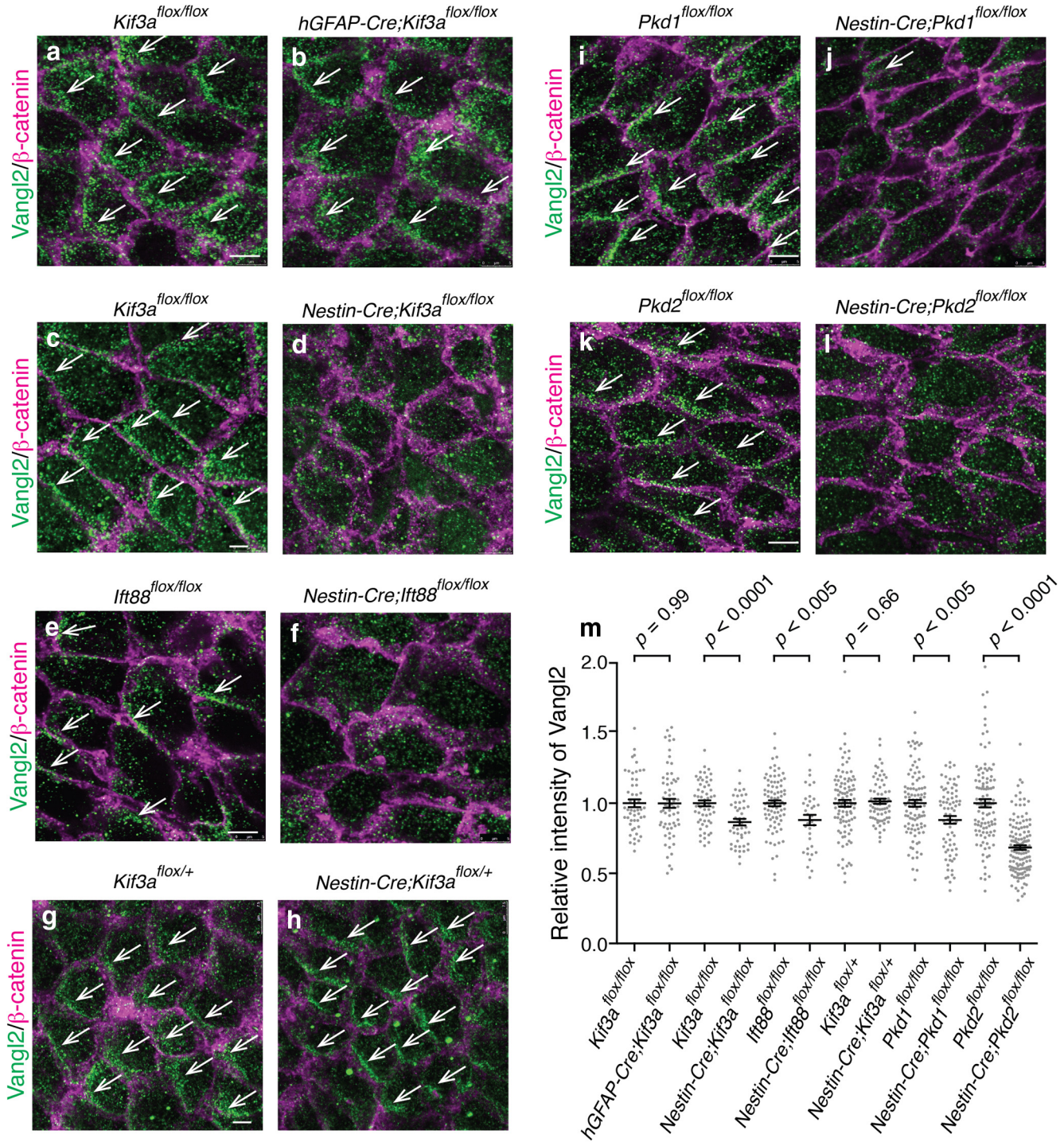

Figure 5. Primary cilia of RGCs, *Pkd1*, and *Pkd2* were required for the asymmetric localization of Vangl2. ***a–l***, Whole-mount preparations of the lateral walls of the lateral ventricle were stained with antibodies against Vangl2 (green) and β-catenin (magenta) in *Kif3a*$^{flox/flox}$ (***a***, sibling control for *hGFAP-Cre;Kif3a*$^{flox/flox}$ in ***b***), *hGFAP-Cre;Kif3a*$^{flox/flox}$ (***b***), *Kif3a*$^{flox/flox}$ (***c***, sibling control for *Nestin-Cre;Kif3a*$^{flox/flox}$ in ***d***), *Nestin-Cre;Kif3a*$^{flox/flox}$ (***d***), *Ift88*$^{flox/flox}$ (***e***), *Nestin-Cre;Ift88*$^{flox/flox}$ (***f***), *Kif3a*$^{flox/+}$ (***g***), *Nestin-Cre;Kif3a*$^{flox/+}$ (***h***), *Pkd1*$^{flox/flox}$ (***i***), *Nestin-Cre;Pkd1*$^{flox/flox}$ (***j***), *Pkd2*$^{flox/flox}$ (***k***), and *Nestin-Cre;Pkd2*$^{flox/flox}$ (***l***) mice at P21. White arrows indicate asymmetric localization of Vangl2. Scale bar, 5 μm. ***m***, Ablation of primary cilia in RGCs, *Pkd1*, or *Pkd2* resulted in a reduction in the apical levels of Vangl2 staining in E cells at P21. Data shown are mean ± SEM. Each point on the graph is relative intensity of Vangl2 immunosignal from an individual E cell. *Kif3a*$^{flox/flox}$ (sibling control for *hGFAP-Cre;Kif3a*$^{flox/flox}$), 51 cells, four mice; *hGFAP-Cre;Kif3a*$^{flox/flox}$, 63 cells, four mice, $p = 0.99$. *Kif3a*$^{flox/flox}$ (sibling control for *Nestin-Cre;Kif3a*$^{flox/flox}$), 57 cells, three mice; *Nestin-Cre;Kif3a*$^{flox/flox}$, 48 cells, three mice, $p < 0.0001$. *Ift88*$^{flox/flox}$, 84 cells, four mice; *Nestin-Cre;Ift88*$^{flox/flox}$, 35 cells, four mice, $p = 0.0035$. *Kif3a*$^{flox/+}$, 98 cells, four mice; *Nestin-Cre;Kif3a*$^{flox/+}$, 71 cells, four mice; $p = 0.66$. *Pkd1*$^{flox/flox}$, 98 cells, five mice; *Nestin-Cre;Pkd1*$^{flox/flox}$, 75 cells, six mice; $p = 0.0013$. *Pkd2*$^{flox/flox}$, 106 cells, six mice; *Nestin-Cre;Pkd2*$^{flox/flox}$, 136 cells, six mice; $p < 0.0001$.

RGCs are required for the asymmetric distribution of Vangl2 in E cells.

As shown in Figures 2 and 3, Pkd1 and Pkd2 were expressed in the primary cilia of RGCs. So we asked whether Pkd1 and Pkd2 were required for Vangl2 asymmetrical localization in the apical area of E cells at P21 (Fig. 5*i–l*). In *Pkd1*$^{flox/flox}$ and *Pkd2*$^{flox/flox}$ control mice, Vangl2 staining was observed in a crescent-shape close to the intercellular junctions on one side of E cells apical membrane (Fig. 5*i*,*k*; *Pkd1*$^{flox/flox}$, 68/95 cells, 5 mice, 72%; *Pkd2*$^{flox/flox}$, 74/128, 4 mice, 58%). In contrast, in the *Nestin-Cre;Pkd1*$^{flox/flox}$ and *Nestin-Cre;Pkd2*$^{flox/flox}$ E cells, this asymmetric accumulation of Vangl2 was not observed (Fig. 5*j*,*l*; *Nestin-Cre;*

Pkd1$^{flox/flox}$,18/93, 6 mice, 19%, $p < 0.0001$; *Nestin-Cre;Pkd2*$^{flox/flox}$, 25/121, 3 mice, 21%, $p < 0.0001$). These results suggest that Pkd1 and Pkd2 are required for Vangl2 asymmetric localization in E cells. Interestingly, the relative intensity of Vangl2-immunosignal in the apical area of E cells was also significantly reduced in *Nestin-Cre;Kif3a*$^{flox/flox}$, *Nestin-Cre;Ift88*$^{flox/flox}$, *Nestin-Cre;Pkd1*$^{flox/flox}$, and *Nestin-Cre;Pkd2*$^{flox/flox}$ mice but not in *Nestin-Cre;Kif3a*$^{flox/+}$ or *hGFAP-Cre;Kif3a*$^{flox/flox}$ mice (Fig. 5*m*). These results suggest that primary cilia of RGCs, Pkd1, or Pkd2 also affect the apical levels of Vangl2 in E cells directly or indirectly.

Aberrant rotational polarity in *Nestin-Cre;Pkd1*$^{flox/flox}$ and *Nestin-Cre;Pkd2*$^{flox/flox}$ mice

To examine the role of *Pkd1* and *Pkd2* in rotational polarity of individual E cells' cilia, we used sequential tangential ultrathin sections and transmission electron microscopy (TEM) to determine the location of the basal foot next to E cells' BBs (Guirao et al., 2010; Hirota et al., 2010; Mirzadeh et al., 2010b). In control animals, the majority of basal feet in E cells were oriented in the same direction, while this rotational polarity was significantly disrupted in *Nestin-Cre;Pkd1*$^{flox/flox}$ and *Nestin-Cre;Pkd2*$^{flox/flox}$ (Fig. 6*a–p*): the total number of cilia oriented in the same direction and the circular SD (CSD) of basal foot orientation (Fig. 6*m–o*, error bars) were significantly disrupted. These results suggest that both *Pkd1* and *Pkd2* are required for the proper alignment of BBs within E cells.

Defects in rotational polarity frequently result in reduced ependymal flow speed and expansion of the ventricles (Guirao et al., 2010; Hirota et al., 2010; Ohata et al., 2014; Ying et al., 2014). The continuous beating of cilia on the apical surface of E cells generates this unidirectional fluid flow (Miyan et al., 2003; Del Bigio, 2010; Lee, 2013), which can be visualized and quantified by placing polystyrene latex fluorescent microbeads on live preparations of the lateral wall of the lateral ventricle (Fig. 6*q*; Sawamoto et al., 2006; Mirzadeh et al., 2010a,b; Ohata et al., 2014). We next investigated the ependymal flow in whole-mount preparations from control, *Nestin-Cre;Pkd1*$^{flox/flox}$, and *Nestin-Cre;Pkd2*$^{flox/flox}$ mice. When a small number of microbeads were placed in the anterior dorsal region of the lateral ventricles in control mice, a strong posterior-dorsal to anterior-ventral current was observed (Fig. 6*r*; Movies 5, 7). In *Nestin-Cre;Pkd1*$^{flox/flox}$ and *Nestin-Cre;Pkd2*$^{flox/flox}$ mice, the overall directionality of this flow was similar to that in controls (Fig. 6*r*; Movies 6, 8), but the speed of the fluorescent beads was significantly slower compared with controls (Fig. 6*s*). *Nestin-Cre;Pkd1*$^{flox/flox}$ mice have been shown to develop hydrocephalus (Wodarczyk et al., 2009). Consistently, the volume of the lateral ventricles was significantly larger in *Nestin-Cre;Pkd2*$^{flox/flox}$ mice compared with *Pkd2*$^{flox/flox}$ mice at P31 (Figure 6*t*,*u*; *Pkd2*$^{flox/flox}$, 0.63 ± 0.067 mm^3; mean ± SEM; $n = 11$; *Nestin-Cre;Pkd2*$^{flox/flox}$, 1.6 ± 0.031 mm^3, $n = 9$, $p = 0.00060$). These results indicate that in mice lacking *Pkd1* or Pkd2, the rotational polarity of basal body, ependymal flow, and the size of the lateral ventricles are abnormal.

Abnormal translational polarity in *Nestin-Cre;Kif3a*$^{flox/flox}$, *Nestin-Cre;Pkd1*$^{flox/flox}$, and *Nestin-Cre;Pkd2*$^{flox/flox}$ mice

Translational polarity is established in RGCs ~E16 (Mirzadeh et al., 2010b; Boutin et al., 2014), and a subpopulation of these RGCs differentiate into E cells by P5 (Spassky et al., 2005). To assess whether primary cilia, *Pkd1*, and *Pkd2* are involved in the establishment of translational polarity in RGCs at P0 (a timepoint before most RGCs differentiate into E cells), we drew vectors from the center of the apical surface to the BB of RGCs in control, *Nestin-Cre;Kif3a*$^{flox/flox}$, *Nestin-Cre;Pkd1*$^{flox/flox}$, and *Nestin-Cre;Pkd2*$^{flox/flox}$ mice (Fig. 7*a–g*). We measured the angles of these vectors (BB angle) and the displacement of the BBs from the center of the apical surface (BB displacement; Fig. 7*a*). BB angle in RGCs at P0 distributed significantly more widely in *Nestin-Cre;Kif3a*$^{flox/flox}$, *Nestin-Cre;Pkd1*$^{flox/flox}$, and *Nestin-Cre;Pkd2*$^{flox/flox}$ mice compared with that in control mice (Fig. 7*b–j*). The BB displacement was significantly smaller in *Nestin-Cre;Kif3a*$^{flox/flox}$, *Nestin-Cre;Pkd1*$^{flox/flox}$, and *Nestin-Cre;Pkd2*$^{flox/flox}$ mice compared with that in control mice (Fig. 7*k*). These data indicate that primary cilia, *Pkd1*, and *Pkd2* contribute to the establishment of translational polarity in RGCs before they differentiate into E cells.

We next investigated whether translational polarity in differentiated E cells at P21 was affected following ablation of *Pkd1* or *Pkd2* using *Nestin-Cre*. The BB patch angle in E cells had a significantly wider distribution in both *Nestin-Cre;Pkd1*$^{flox/flox}$ and *Nestin-Cre;Pkd2*$^{flox/flox}$ compared with controls (Figs. 4*k–n*, 8*a–f*). However, E cells' BB patch displacement was not significantly different between control and *Nestin-Cre;Pkd1*$^{flox/flox}$, or *Nestin-Cre;Pkd2*$^{flox/flox}$ mice (Fig. 8*g*). These results suggest that *Pkd1* and *Pkd2* help coordinate BB patch angle in E cells.

Synergistic enhancement of PCP defects in the *Vangl2* heterozygous mutant E cells by *Pkd1* heterozygous mutation

In the developing kidney epithelia, ablation of *Pkd1* affects multiple cellular processes related to PCP, including oriented cell division and convergent-extension-like movements (Luyten et al., 2010; Castelli et al., 2013). However, whether and how Pkd1 regulates the PCP pathway remains unknown. The PCP gene *Vangl2* is required for both rotational and translational polarity in E cells (Guirao et al., 2010; Boutin et al., 2014). The *Loop-tail* mutation (*Vangl2*^{Lp}, S464N) affects the stability and membrane localization of Vangl2 (Montcouquiol et al., 2006; Guirao et al., 2010; Merte et al., 2010; Iliescu et al., 2011). To address whether *Pkd1* and *Vangl2* function cooperatively or independently in the establishment of translational and rotational polarity, we analyzed single and double-heterozygous mutant mice for these genes. Heterozygous *Vangl2*$^{Lp/+}$ mutation was sufficient to significantly affect the BB patch angle in E cells at P21 (Fig. 9*a*,*b*,*e*; Table 1). In contrast, the BB patch angle was unaffected in *Nestin-Cre;Pkd1*$^{flox/+}$ mice compared with *Pkd1*$^{flox/+}$ mice (Fig. 9*a*,*c*,*e*; Table 1). If *Pkd1* and *Vangl2* were to function independently, double-heterozygous mutations of *Pkd1* and *Vangl2* in *Nestin-Cre;Pkd1*$^{flox/+}$;*Vangl2*$^{Lp/+}$ mice should result in an additive effect on the randomization of BB patch angle (*i*.e., similar effects to those observed in *Vangl2*$^{Lp/+}$ mutants). However, we observed a synergistic effect on the disorientation of BB patch angle by double-heterozygous mutations for *Pkd1* and *Vangl2* in *Nestin-Cre;Pkd1*$^{flox/+}$;*Vangl2*$^{Lp/+}$ mice compared with *Pkd1* single heterozygous mice (*Nestin-Cre;Pkd1*$^{flox/+}$) or *Vangl2* single heterozygous mice (*Pkd1*$^{flox/+}$;*Vangl2*$^{Lp/+}$) individually (Fig. 9*b–e*; Table 1). These results suggest that *Pkd1* and *Vangl2* function in the same pathway to coordinate BB patch angle.

Next, we examined rotational polarity in these mutant mice. Both *Pkd1* and *Vangl2* heterozygous mutations affected rotational polarity (Fig. 9*f–h*,*j*; Table 2). The difference in CSD between *Nestin-Cre;Pkd1*$^{flox/+}$ mice and *Pkd1*$^{flox/+}$ mice was 8° (48° and 40°, respectively) and that between *Pkd1*$^{flox/+}$;*Vangl2*$^{Lp/+}$ mice and *Pkd1*$^{flox/+}$ mice was 9° (49° and 40°, respectively). Interestingly, double-heterozygous mutant mice for these genes

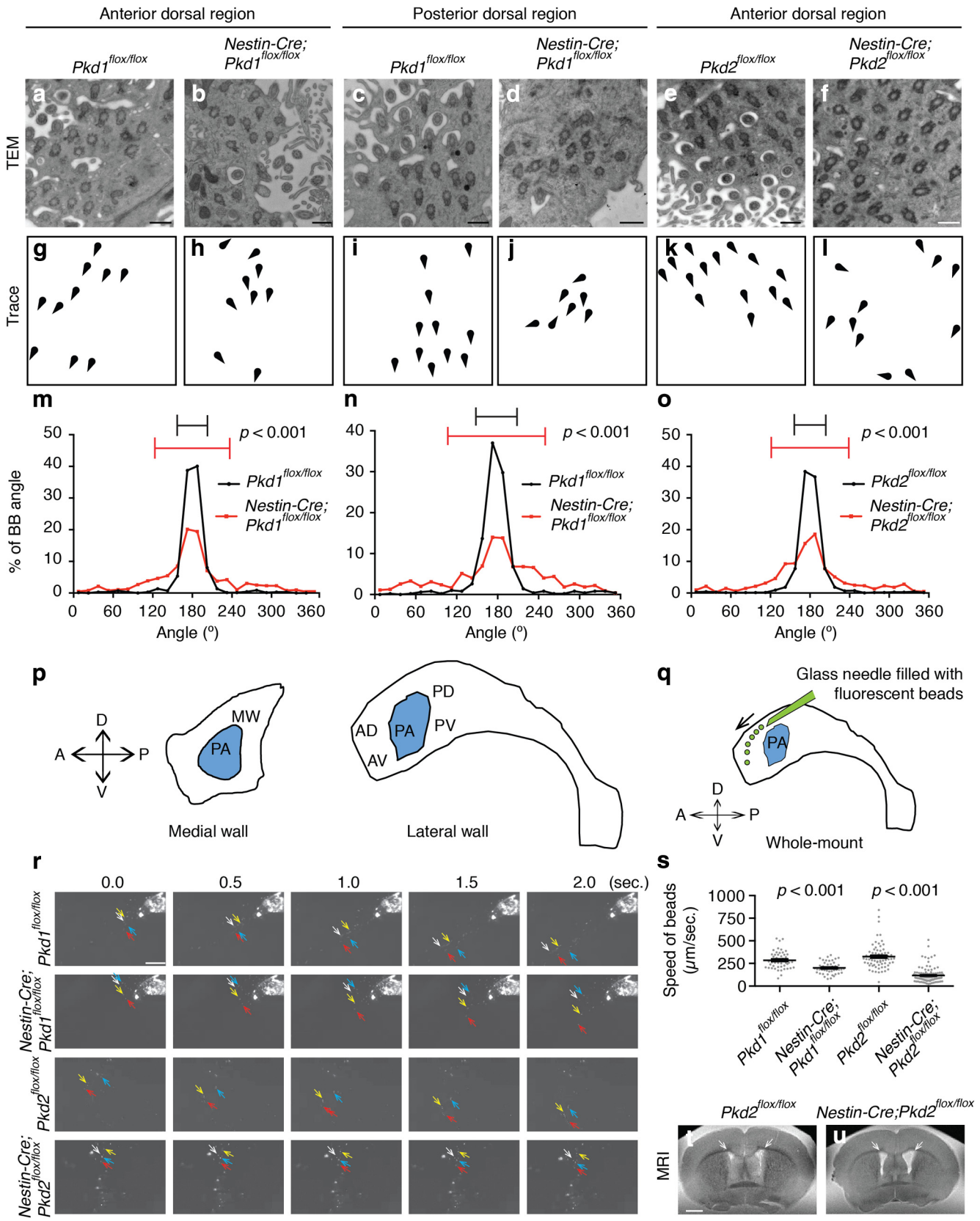

Figure 6. Rotational polarity was disrupted in the *Nestin-Cre;Pkd1*$^{flox/flox}$ and *Nestin-Cre;Pkd2*$^{flox/flox}$ E cells. ***a–f***, TEM analysis of rotational polarity in E cells in the anterior-dorsal region in *Pkd1*$^{flox/flox}$ (***a***), *Nestin-Cre;Pkd1*$^{flox/flox}$ (***b***), *Pkd2*$^{flox/flox}$ (***e***), and *Nestin-Cre;Pkd2*$^{flox/flox}$ (***f***) mice, and in the posterior dorsal region in *Pkd1*$^{flox/flox}$ (***c***) and *Nestin-Cre;Pkd1*$^{flox/flox}$ (***d***) mice at P21. See Figure 6*p* for the annotation of anterior dorsal and posterior dorsal regions. Scale bar, 500 nm. ***g–l***, Schematic drawings of BBs shown in a-f illustrate the misalignment of BB rotational orientation in *Nestin-Cre;Pkd1*$^{flox/flox}$ and *Nestin-Cre;Pkd2*$^{flox/flox}$ mice. ***m–o***, Histogram showing the distribution of the BB angle in the *Pkd1*$^{flox/flox}$ (***m***, black; CSD = 23°; $n = 674$ BBs from 74 cells, three mice), *Nestin-Cre;Pkd1*$^{flox/flox}$ (***m***, red; CSD = 57°; $n = 1116$ BBs from 101 cells, three mice; $p < 0.001$), *Pkd2*$^{flox/flox}$ (***o***, black; CSD = 24°; $n = 1575$ BBs from 141 cells, five mice), and *Nestin-Cre;Pkd2*$^{flox/flox}$ (***o***, red; CSD = 59°; $n = 607$ BBs from 76 cells, four mice; $p < 0.001$) E cells in the anterior dorsal region, and in the *Pkd1*$^{flox/flox}$ (***n***, black; CSD = 30°; (*Figure legend continues.*)

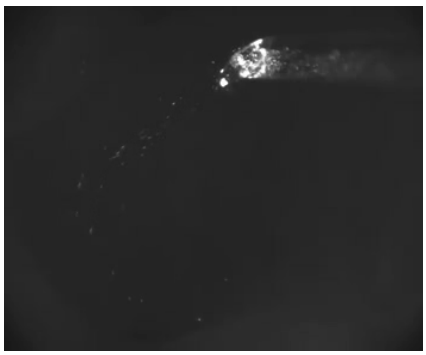

Movies 5. Live imaging movie showing the migration of fluorescent beads on the whole-mount preparation of lateral wall of lateral ventricle in *Pkd1* $^{flox/flox}$ mouse.

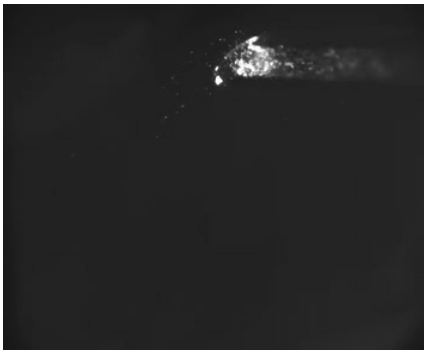

Movies 6. Live imaging movie showing ciliary beating of E cells in *Nestin-Cre;Pkd1* $^{flox/flox}$ mouse.

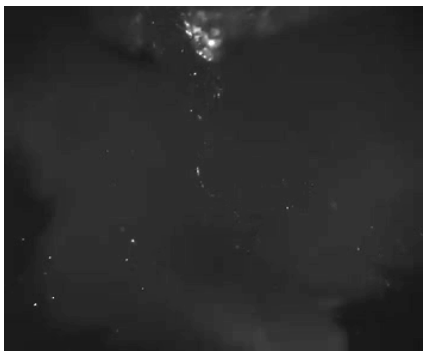

Movies 7. Live imaging movie showing the migration of fluorescent beads on the whole-mount preparation of lateral wall of lateral ventricle in *Pkd2* $^{flox/flox}$ mouse.

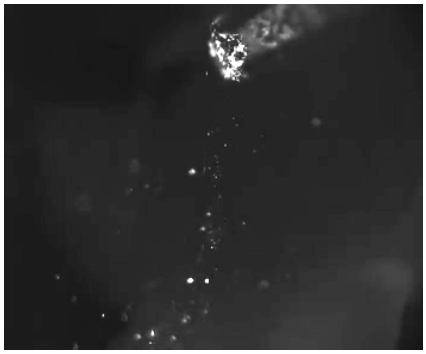

Movies 8. Live imaging movie showing ciliary beating of E cells in *Nestin-Cre;Pkd2* $^{flox/flox}$ mouse.

(*Nestin-Cre;Pkd1*$^{flox/+}$;*Vangl2*$^{Lp/+}$) displayed more severe defect in rotational polarity than that of *Nestin-Cre;Pkd1*$^{flox/+}$ or *Pkd1*$^{flox/+}$;*Vangl2*$^{Lp/+}$ mice (Fig. 9*g–j*; Table 2). The difference in CSD between *Nestin-Cre;Pkd1*$^{flox/+}$;*Vangl2*$^{Lp/+}$ mice and *Pkd1*$^{flox/+}$ mice was 32° (72° and 40°, respectively), almost twice the sum of the differences in CSD for *Nestin-Cre;Pkd1*$^{flox/+}$ and *Pkd1*$^{flox/+}$;*Vangl2*$^{Lp/+}$ mice (8° and 9°, respectively). As with translational polarity, these results for rotational polarity suggest that *Pkd1* and *Vangl2* do not function independently, but are part of the same pathway to establish PCP in E cells.

←

(*Figure legend continued.*) $n = 497$ BBs from 68 E cells, three mice) and *Nestin-Cre;Pkd1*$^{flox/flox}$ (***n***, red; CSD = 55°; $n = 543$ BBs, 55 E cells, three mice; $p < 0.001$) E cells in the posterior dorsal region. Error bars on the graphs show CSD. ***p***, Schematic drawing of the regions of the lateral and medial walls of the lateral ventricle studied in the present study. A, Anterior; D, dorsal; P, posterior; V, ventral. AD, anterior dorsal; AV, anterior ventral; MW, medial wall; PA, point of adhesion; PD, posterior dorsal; PV, posterior ventral. ***q–s***, The speed of ependymal flow was significantly slower in *Nestin-Cre;Pkd1*$^{flox/flox}$ and *Nestin-Cre;Pkd2*$^{flox/flox}$ mice at P21. ***q***, Schematic of the ependymal flow assay. Fluorescent beads (green) were filled in a glass needle and placed onto whole-mount preparations of the lateral walls of lateral ventricle. A, Anterior; D, dorsal; P, posterior; PA, point of adhesion; V, ventral. ***r***, Migration patterns of the fluorescent beads placed on the whole-mount preparations of the lateral walls of lateral ventricle in *Pkd1*$^{flox/flox}$ (top row), *Nestin-Cre;Pkd1*$^{flox/flox}$ mutant (second top row), *Pkd2*$^{flox/flox}$ (second bottom row), and *Nestin-Cre;Pkd2*$^{flox/flox}$ mutant (bottom row) mice. The arrows indicate the position of arbitrarily chosen fluorescent beads. Scale bar, 50 μm. ***s***, The speeds of fluorescent beads on the whole-mount preparation are expressed as mean ± SEM. Each point on the graph represents the speed of individual fluorescent beads. *Pkd1*$^{flox/flox}$; $n = 102$ beads, four mice. *Nestin-Cre;Pkd1*$^{flox/flox}$; $n = 120$ beads, five mice. $p < 0.0001$. *Pkd2*$^{flox/flox}$; $n = 70$ beads, five mice. *Nestin-Cre;Pkd2*$^{flox/flox}$; $n = 115$ beads, four mice. $p < 0.0001$ (Movies 5–8). ***t***, ***u***, T2-weighted coronal MRI scans showing enlargement of the lateral ventricles in *Nestin-Cre;Pkd2*$^{flox/flox}$ mice (***u***) compared with *Pkd2*$^{flox/flox}$ mice (***t***) at P31. White arrows point the lateral ventricles. Scale bar, 1 mm.

Discussion

The present study demonstrates that the planar organization of E cells, essential for the proper CSF circulation, requires RGCs' primary cilia and mechanosensory genes, *Pkd1* and *Pkd2*. Together with our previous report (Mirzadeh et al., 2010b), we propose that Pkd1 and Pkd2 in the primary cilia of RGCs could help sense small perturbations in early hydrodynamic forces on the ventricular epithelium (e.g., passive CSF flow) to establish an initial translational polarity in RGCs. Given that E cells' PCP in *Pkd1* mutant mice was affected in all ventricular wall subdomains, this planar polarization mechanism may be widely used along the ventricular epithelium. How this early polarization of RGCs is then translated into polarized E cells remains unknown. During differentiation of RGCs to E cells, newly generated BBs for motile cilia migrate apically into the vicinity of the primary cilia's BBs (Al Jord et al., 2014). The asymmetric localizations of the primary cilia and its BBs in RGCs may be key for the subsequent asymmetric positioning of motile cilia and BBs in E cells.

Ciliary localization of Pkd1 and Pkd2 in RGCs

Primary cilium compartmentalizes membrane-bound and cytoplasmic signaling components and functions as a signaling center for chemical and mechanical signals (Nauli et al., 2003; Su et al., 2013; Guemez-Gamboa et al., 2014; Lee et al., 2015). Here we show that mechanoreceptor proteins Pkd1 and Pkd2 are present in RGCs' primary cilia, which extend into the developing ventricular system and contact the CSF directly (Mirzadeh et al., 2010b; Tong et al., 2014). The elongated shape of the primary cilium and the compartmentalization of Pkd1 and Pkd2 within its small volume could enable the primary cilium to function as a highly sensitive mechanosensory organelle.

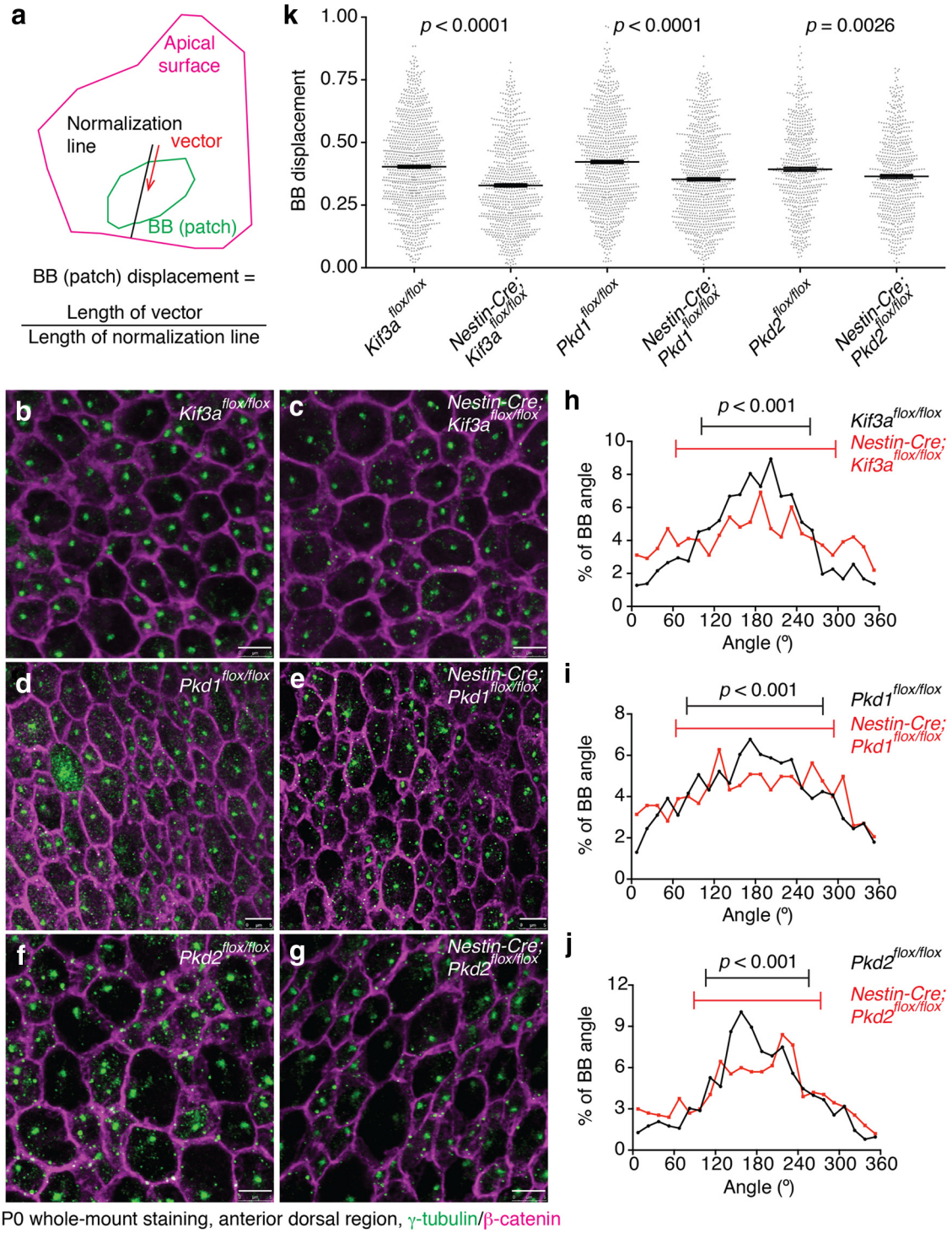

Figure 7. Primary cilia, *Pkd1*, and *Pkd2* were involved in the establishment of translational polarity in RGCs. ***a***, Schematic drawing showing BB patch angle and BB patch displacement. A vector (red arrow) was drawn from the center of apical surface to that of BB patch (in case of RGCs, BBs of primary cilia). To calculate BB patch displacement, the length of the vector was normalized with the length of the line extended to the edge of the apical surface (black line). ***b–g***, Whole-mount preparations of the lateral walls of the lateral ventricle at P0 were stained with antibodies against γ-tubulin (green) and β-catenin (magenta) in *Kif3a*$^{flox/flox}$ (***b***), *Nestin-Cre;Kif3a*$^{flox/flox}$ (***c***), *Pkd1*$^{flox/flox}$ (***d***), *Nestin-Cre;Pkd1*$^{flox/flox}$ (***e***), *Pkd2*$^{flox/flox}$ (***f***), and *Nestin-Cre;Pkd2*$^{flox/flox}$ (***g***) mice. Scale bar, 5 μm. ***h–j***, Histogram showing the distribution of BB angles in *Kif3a*$^{flox/flox}$ (***h***, black; CSD = 79°; $n = 1018$ RGCs, five mice), *Nestin-Cre;Kif3a*$^{flox/flox}$ (***h***, red; CSD = 116°; $n = 997$ RGCs, five mice; $p < 0.001$), *Pkd1*$^{flox/flox}$ (***i***, black; CSD = 99°; $n = 1225$ RGCs, eight mice) and *Nestin-Cre;Pkd1*$^{flox/flox}$ (***i***, red; CSD = 115°; $n = 924$ RGCs, five mice; $p < 0.001$), *Pkd2*$^{flox/flox}$ (***j***, black; CSD = 75°; $n = 627$ RGCs, four mice) and *Nestin-Cre;Pkd2*$^{flox/flox}$ (***j***, red; CSD = 92°; $n = 667$ RGCs, four mice; $p < 0.001$) mice at P0. Error bars on the graph show CSD. ***k***, Quantification of BB displacement. Data shown are mean ± SEM. Each point on the graphs is BB displacement of an individual RGC or E cell. *Kif3a*$^{flox/flox}$; $n = 1125$ RGCs, five mice: *Nestin-Cre; Kif3a*$^{flox/flox}$; $n = 852$ RGCs, five mice; $p < 0.0001$. *Pkd1*$^{flox/flox}$; $n = 948$ RGCs, six mice: *Nestin-Cre;Pkd1*$^{flox/flox}$; $n = 927$ RGCs, five mice; $p < 0.0001$. *Pkd2*$^{flox/flox}$; $n = 600$ RGCs, four mice: *Nestin-Cre;Pkd2*$^{flox/flox}$; $n = 657$ RGCs, four mice; $p = 0.0026$.

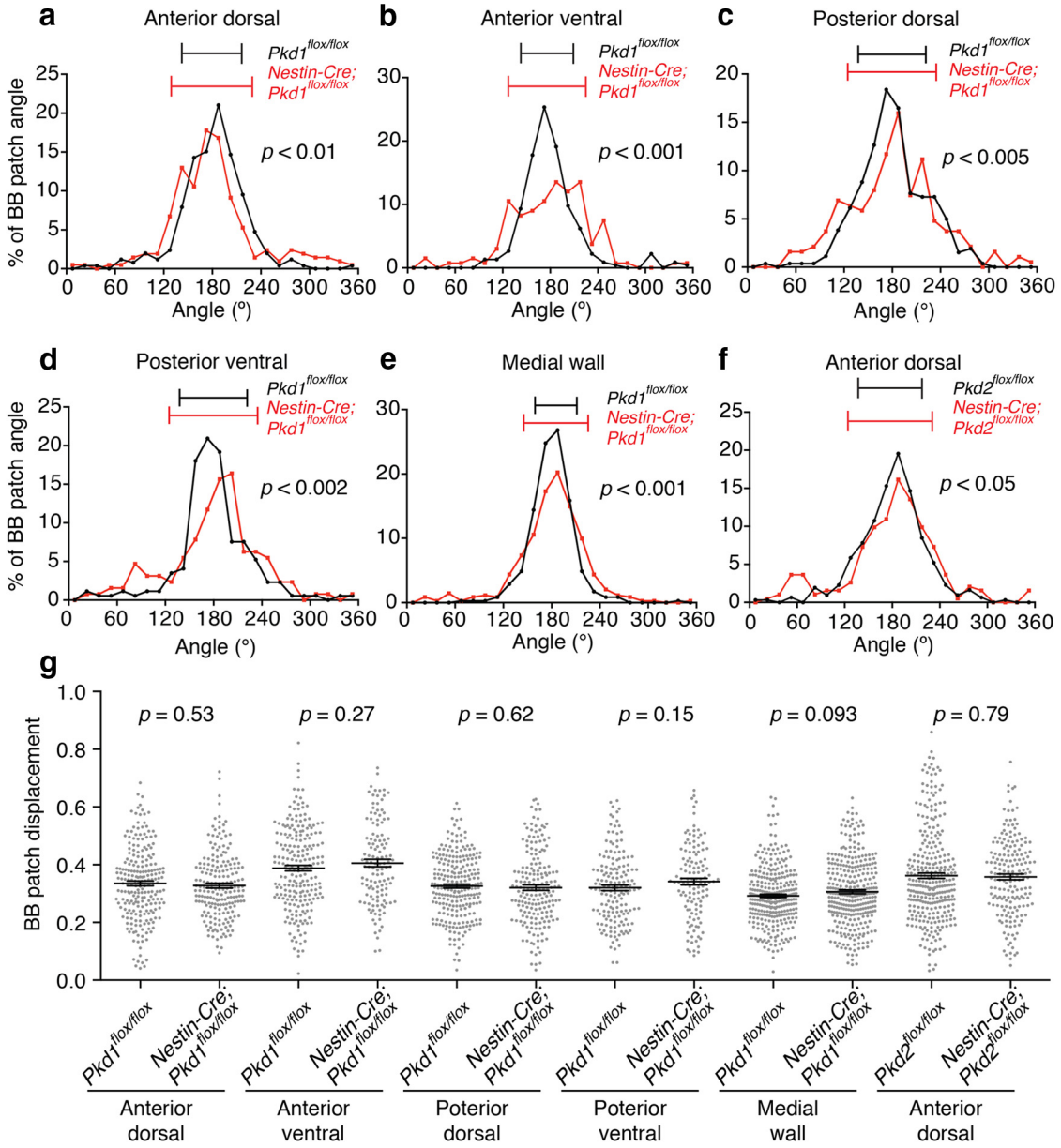

Figure 8. *Pkd1* and *Pkd2* contributed to translational polarity in E cells. ***a–f***, Histograms showing the distribution of the BB patch angles in the *Pkd1*$^{flox/flox}$ (***a–e***, black), *Nestin-Cre;Pkd1*$^{flox/flox}$ (***a–e***, red), *Pkd2*$^{flox/flox}$ (***f***, black), and *Nestin-Cre;Pkd2*$^{flox/flox}$ (***f***, red) E cells in the anterior dorsal (***a***, ***f***), anterior ventral (***b***), posterior dorsal (***c***), and posterior ventral (***d***) regions of the lateral wall and medial wall (***e***) of the lateral ventricle. Error bars on the graph show CSD. ***a***, *Pkd1*$^{flox/flox}$; CSD = 37°, $n = 252$ E cells, three mice. *Nestin-Cre;Pkd1*$^{flox/flox}$; CSD = 50°, $n = 208$ E cells, four mice; $p < 0.01$. ***b***, *Pkd1*$^{flox/flox}$; CSD = 34°, $n = 225$ E cells, three mice. *Nestin-Cre;Pkd1*$^{flox/flox}$; CSD = 49°, $n = 133$ E cells, three mice; $p < 0.001$. ***c***, *Pkd1*$^{flox/flox}$, CSD = 42°, $n = 261$ E cells, three mice; *Nestin-Cre;Pkd1*$^{flox/flox}$, CSD = 55°, $n = 188$ E cells, three mice; $p < 0.005$. ***d***, *Pkd1*$^{flox/flox}$, CSD = 42°, $n = 172$ E cells, three mice; *Nestin-Cre;Pkd1*$^{flox/flox}$, CSD = 55°, $n = 128$ E cells, three mice; $p < 0.002$. ***e***, *Pkd1*$^{flox/flox}$, CSD = 26°, $n = 347$ E cells, three mice; *Nestin-Cre;Pkd1*$^{flox/flox}$, CSD = 40°, $n = 341$ E cells, three mice; $p < 0.001$. ***f***, *Pkd2*$^{flox/flox}$; CSD = 40°; $n = 307$ E cells, three mice: *Nestin-Cre;Pkd2*$^{flox/flox}$; CSD = 53°; $n = 192$ E cells, three mice; $p < 0.05$. See Figure 6*p* for the annotation of regions examined in the present study. ***g***, Quantification of BB patch displacement. Data shown are mean ± SEM. Each point on the graphs is BB patch displacement of an individual E cell. Anterior dorsal region: *Pkd1*$^{flox/flox}$; $n = 222$ E cells, three mice: *Nestin-Cre;Pkd1*$^{flox/flox}$; $n = 197$ E cells, four mice: $p = 0.53$. Anterior ventral region: *Pkd1*$^{flox/flox}$; $n = 219$ E cells, three mice: *Nestin-Cre;Pkd1*$^{flox/flox}$; $n = 126$ E cells, three mice: $p = 0.27$. Posterior dorsal region: *Pkd1*$^{flox/flox}$; $n = 250$ E cells, three mice: *Nestin-Cre;Pkd1*$^{flox/flox}$; $n = 186$ E cells, three mice: $p = 0.62$. Posterior ventral region: *Pkd1*$^{flox/flox}$; $n = 162$ E cells, three mice: *Nestin-Cre;Pkd1*$^{flox/flox}$; $n = 124$ E cells, three mice: $p = 0.15$. Medial wall: *Pkd1*$^{flox/flox}$, $n = 309$ E cells, three mice: *Nestin-Cre;Pkd1*$^{flox/flox}$, $n = 320$ E cells, three mice: $p = 0.093$. Anterior dorsal region: *Pkd2*$^{flox/flox}$; $n = 307$ E cells, three mice: *Nestin-Cre;Pkd2*$^{flox/flox}$; $n = 184$ E cells, three mice: $p = 0.79$. See Figure 6*p* for the annotation of regions examined in the present study.

Pkd1 and Pkd2 were also present as small puncta in the apical compartment of RGCs. A possible role for these mechanosensors in the apical region remains unknown. In vascular smooth muscle, these proteins localize on the apical surface and are involved in sensing pressure generated by the stretching of the plasma membrane (Sharif-Naeini et al., 2009). Apical Pkd1 and Pkd2, outside the cilia, could have a similar function in RGCs. It is also possible that the punctate staining we detect in the apical domain of RGCs corresponds to Pkd1 or Pkd2 being transported or recycled.

Regulation of PCP pathway by Pkd1, Pkd2, and primary cilia

In the present study, we show that primary cilia, Pkd1, and Pkd2 are required for the asymmetric localization of Vangl2, a core PCP protein essential for planar polarization of E cells (Guirao et

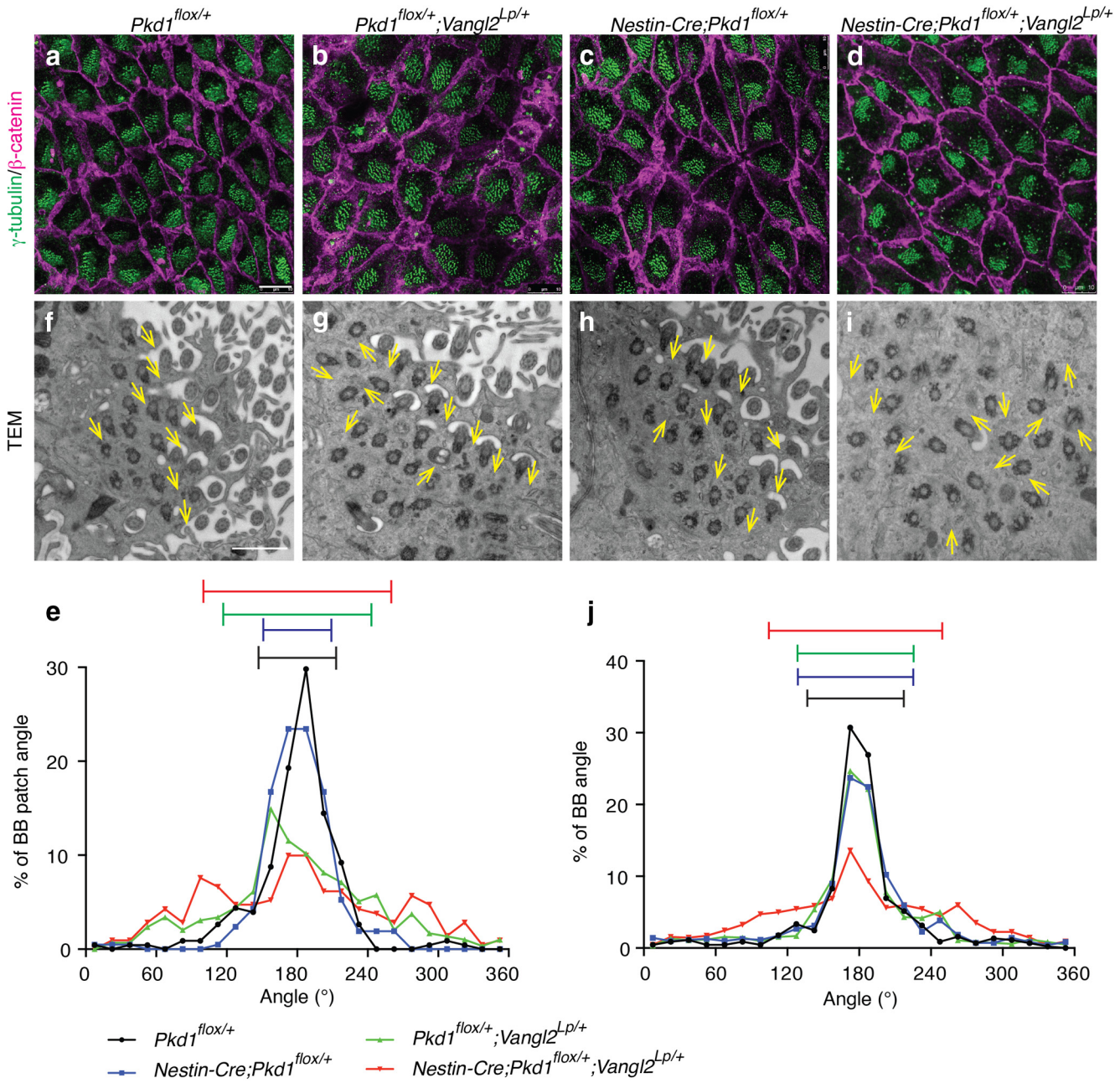

Figure 9. *Pkd1* and *Vangl2* functioned in the same pathway to coordinate BB patch angle and rotational alignment of BBs in E cells. ***a–d***, Whole-mount preparations of the lateral walls of the lateral ventricle at P21 were stained with antibodies against γ-tubulin (green) and β-catenin (magenta) in *Pkd1*$^{flox/+}$ (***a***), *Pkd1*$^{flox/+}$;*Vangl2*$^{Lp/+}$ (***b***), *Nestin-Cre;Pkd1*$^{flox/+}$ (***c***), and *Nestin-Cre;Pkd1*$^{flox/+}$;*Vangl2*$^{Lp/+}$ (***d***) mice. E cells in the anterior dorsal region were analyzed. Scale bars, 10 μm. ***e***, Histograms showing the distribution of the BB patch angles in *Pkd1*$^{flox/+}$ (black; CSD = 33°; n = 228 E cells, three mice), *Nestin-Cre;Pkd1*$^{flox/+}$ (blue; CSD = 29°; n = 209 E cells, three mice), *Pkd1*$^{flox/+}$;*Vangl2*$^{Lp/+}$ (green; CSD = 63°; n = 295 E cells, three mice), and *Nestin-Cre;Pkd1*$^{flox/+}$;*Vangl2*$^{Lp/+}$ (red; CSD = 77°; n = 211 E cells, three mice) mice. Error bars on the graph show CSD. ***f–i***, TEM analysis of rotational polarity in *Pkd1*$^{flox/+}$ (***f***), *Pkd1*$^{flox/+}$;*Vangl2*$^{Lp/+}$ (***g***), *Nestin-Cre;Pkd1*$^{flox/+}$ (***h***), and *Nestin-Cre;Pkd1*$^{flox/+}$;*Vangl2*$^{Lp/+}$ (***i***) mice. E cells in the anterior dorsal region were analyzed. Scale bar, 1 μm. Yellow arrows indicate the directions of individual BBs. ***j***, Histogram showing the distribution of the rotational angle of BBs in the *Pkd1*$^{flox/+}$ (black; CSD = 40°; n = 446 BBs from 55 cells, three mice), *Nestin-Cre;Pkd1*$^{flox/+}$ (blue; CSD = 48°; n = 704 BBs from 68 E cells, three mice), *Pkd1*$^{flox/+}$;*Vangl2*$^{Lp/+}$ (green; CSD = 49°; n = 835 BBs from 81 E cells, three mice), and *Nestin-Cre;Pkd1*$^{flox/+}$;*Vangl2*$^{Lp/+}$ (red; CSD = 72°; n = 1104 BBs from 102 E cells, three mice) E cells. Error bars on the graph show CSD.

al., 2010; Boutin et al., 2014). The double-heterozygous mutant experiments suggest that *Pkd1* and *Vangl2* function in the same pathway for both rotational and translational polarity in E cells. Pkd1 and Pkd2 in RGCs' primary cilia may control E cell PCP through the regulation of the asymmetric localization of Vangl2. Our results suggest a molecular link between the hydrodynamic forces created by CSF movements on the ventricular surface of RGCs and the planar polarization within this wall. An alternative, but not mutually exclusive, possibility is that Pkd1 and Pkd2 participate in the sensing of gradients of unknown soluble factors in the CSF. For example, Pkd2 family protein Pkd2-like1 (Pkd2l1) can enhance Sonic hedgehog signaling (Delling et al., 2013). Gradients of secreted factors could help modulate PCP in RGCs.

It remains unclear how primary cilia, Pkd1, and Pkd2 are involved in the establishment of the asymmetric positioning of

Table 1. *p* values for the comparison of BB patch angles by Watson's U^2 test

	Pkd1$^{flox/+}$	*Nestin-Cre; Pkd1*$^{flox/+}$	*Pkd1*$^{flox/+}$*; Vangl2*$^{Lp/+}$	*Nestin-Cre; Pkd1*$^{flox/+}$*; Vangl2*$^{Lp/+}$
Pkd1$^{flox/+}$	—	$0.05 < p < 0.1$	$p < 0.001$	$p < 0.001$
Nestin-Cre;Pkd1$^{flox/+}$	$0.05 < p < 0.1$	—	$p < 0.001$	$p < 0.001$
Pkd1$^{flox/+}$*;Vangl2*$^{Lp/+}$	$p < 0.001$	$p < 0.001$	—	$p < 0.002$
Nestin-Cre;Pkd1$^{flox/+}$*; Vangl2*$^{Lp/+}$	$p < 0.001$	$p < 0.001$	$p < 0.002$	—

p values comparing the distribution of BB patch angle shown in Fig. 9*e*.

Table 2. *p* values for the comparison of BB angles by Watson's U^2 test

	Pkd1$^{flox/+}$	*Nestin-Cre; Pkd1*$^{flox/+}$	*Pkd1*$^{flox/+}$*; Vangl2*$^{Lp/+}$	*Nestin-Cre; Pkd1*$^{flox/+}$*; Vangl2*$^{Lp/+}$
Pkd1$^{flox/+}$	—	$p < 0.001$	$p < 0.001$	$p < 0.001$
Nestin-Cre;Pkd1$^{flox/+}$	$p < 0.001$	—	$0.2 < p < 0.5$	$p < 0.001$
Pkd1$^{flox/+}$*;Vangl2*$^{Lp/+}$	$p < 0.001$	$0.2 < p < 0.5$	—	$p < 0.001$
Nestin-Cre;Pkd1$^{flox/+}$*; Vangl2*$^{Lp/+}$	$p < 0.001$	$p < 0.001$	$p < 0.001$	—

p values comparing the distribution of BB angle shown in Fig. 9*j*.

PCP proteins. In the present study, we show that primary cilia, Pkd1, and Pkd2 contribute to the translational polarity in RGCs. Interestingly, translational polarity in RGCs is observed as early as E16.5, preceding the asymmetric accumulation of PCP proteins that occurs after P0 (Mirzadeh et al., 2010b; Boutin et al., 2014). Positionally biased signaling mediated by primary cilia in RGCs may be important for directional sorting of PCP proteins along microtubules. In the developing fly wing, GFP-tagged Frizzled (Fzd), another core PCP protein, is preferentially transported toward the distal side along microtubule arrays to establish its asymmetric accumulation (Shimada et al., 2006). The BBs of RGCs' primary cilia function as microtubule organizing center (Boutin et al., 2014). Pharmacological disruption of microtubule organization significantly affects the asymmetric localization of core PCP proteins in RGCs and cultured tracheal epithelial cells (Vladar et al., 2012; Boutin et al., 2014). Pkd1 is involved in the stabilization of microtubules in cultured cells (Castelli et al., 2015). Mechanosensory signals may contribute to the initial rearrangement of the apical microtubule networks in RGCs. Proper asymmetric accumulation of PCP proteins in the apical area of RGCs would be important to refine PCP and ultimately instructive for E cells. We also found that ablation of cilia, *Pkd1*, or *Pkd2* resulted in a reduction in apical Vangl2 levels in E cells. Primary cilia of RGCs, *Pkd1*, or *Pkd2*, may directly or indirectly affect synthesis, stability, and/or apical migration of Vangl2.

The requirement of cilia, Pkd1, and Pkd2 in the asymmetric localization of core PCP proteins may be tissue-dependent. The asymmetric accumulation of Vangl2-GFP fusion protein or Fzd3 was not affected in the cochlear hair cells in *Foxg1-Cre;Ift88*$^{flox/flox}$ mice (Jones et al., 2008). In the *Foxg1-Cre;Kif3a*$^{flox/flox}$ cochlea, the asymmetric localizations of Fzd3 and Dishvelled2 are slightly disorganized but largely normal (Sipe and Lu, 2011). Ablation of *Pkd1* in the inner ear disrupts the ultrastructure of actin-based stereocilia but does not affect its PCP (Steigelman et al., 2011).

Primary cilia apparently have different functions at different times in development (Guemez-Gamboa et al., 2014). The early removal of primary cilia, *Pkd1*, or *Pkd2* from RGCs affects the establishment of PCP in RGCs and E cells, whereas late removal of motile cilia from developing E cells partially disrupt E cells' PCP (Mirzadeh et al., 2010b). The early ablation of Arl13b (a small GTPase essential for ciliary function), before neuroepithelial cells convert into RGCs, dramatically reverses apical-basal polarity, whereas its late ablation does not (Higginbotham et al., 2013). Primary cilia may become essential for PCP as the size of the apical area expands in late RGCs.

Partial polarization in *Pkd1* or *Pkd2 mutant mice*

Although PCP in RGCs and E cells were affected in *Nestin-Cre; Pkd1*$^{flox/flox}$ and *Nestin-Cre;Pkd2*$^{flox/flox}$ mice, partial translational and rotational polarity were preserved. Members of the *Pkd1* and *Pkd2* gene families (*Pkd1-like 1,2,3* and *Pkd2-like1,2*; *Pkd1l1,2,3* and *Pkd2l1,2*, respectively; Zhou, 2009) could contribute to this remaining PCP. It has been suggested, in the mouse node and in fish Kupffer's vesicle, that Pkd1l1 interacts with Pkd2 and functions as a nodal flow sensor to establish left-right asymmetry (Field et al., 2011; Kamura et al., 2011). In future studies, it will be interesting to determine the precise localization of the different Pkd1 and Pkd2 protein family members in RGCs and E cells. Compound mutant animals could also help determine the contribution of each *Pkd1* and *Pkd2* family members in the development of PCP in the brain's ventricular epithelium.

We observed a defect in BB displacement in RGCs in *Nestin-Cre;Pkd1*$^{flox/flox}$ or *Nestin-Cre;Pkd2*$^{flox/flox}$ mice at P0, but in these mutant mice, BB patch displacement in E cells was unaffected by P21. As translational polarity is refined during the differentiation and maturation of RGCs into E cells (Mirzadeh et al., 2010b; Boutin et al., 2014; Ohata et al., 2014), the products of Pkd1's and Pkd2's family genes may function in this refinement. It is also possible that the refinement of BB patch displacement during the maturation of E cells is regulated by a different mechanism that does not require Pkd1 or Pkd2.

In *Pkd1* heterozygous mutant mice (i.e., *Nestin-Cre;Pkd1*$^{flox/+}$), partial defects in rotational polarity were observed. Heterozygous mutations in human, which are implicated in autosomal dominant polycystic kidney disease (Zhou, 2009), could be a risk factor for the development of hydrocephalus.

Conclusion

PCP in E cells plays key roles in the proper circulation of CSF and its defects can cause hydrocephalus (Boutin et al., 2014; Ohata et al., 2014; Ying et al., 2014). The present study shows that Pkd1 and Pkd2 are present in the primary cilia of RGCs and are involved in the development of PCP in RGCs and E cells. Hydrodynamic forces have been suggested to guide the development of PCP in E cells and multiciliated cells in the frog larval skin (Mitchell et al., 2007; Guirao et al., 2010; Mirzadeh et al., 2010b). Pkd1 and Pkd2 are involved in mechanosensation in cultured kidney epithelial cells and the embryonic node (Nauli et al., 2003; Yoshiba et al., 2012). Similarly, Pkd1 and Pkd2 could help sense hydrodynamic force in RGCs or immature E cells for the establishment and refinement of proper PCP. The disruption in E cells' PCP in *Nestin-Cre;Pkd1*$^{flox/flox}$ and *Nestin-Cre;Pkd2*$^{flox/flox}$ mice result in abnormal CSF circulation, as shown by slower ependymal flow, and expansion of the lateral ventricles. A full understanding of the mechanism leading to the intricate planar polarization of E cells, which varies by location in the ventricular wall, could help develop genetic tools for the diagnosis and treatment of hydrocephalus. This study identifies molecular components that could mediate mechanosensation in RGCs and E cells.

References

Al Jord A, Lemaître AI, Delgehyr N, Faucourt M, Spassky N, Meunier A (2014) Centriole amplification by mother and daughter centrioles differs in multiciliated cells. Nature 516:104–107. CrossRef Medline

Boutin C, Labedan P, Dimidschstein J, Richard F, Cremer H, André P, Yang Y, Montcouquiol M, Goffinet AM, Tissir F (2014) A dual role for planar cell polarity genes in ciliated cells. Proc Natl Acad Sci U S A 111:E3129–E3138. CrossRef Medline

Castelli M, Boca M, Chiaravalli M, Ramalingam H, Rowe I, Distefano G, Carroll T, Boletta A (2013) Polycystin-1 binds Par3/aPKC and controls convergent extension during renal tubular morphogenesis. Nat Commun 4:2658. CrossRef Medline

Castelli M, De Pascalis C, Distefano G, Ducano N, Oldani A, Lanzetti L, Boletta A (2015) Regulation of the microtubular cytoskeleton by polycystin-1 favors focal adhesions turnover to modulate cell adhesion and migration. BMC Cell Biol 16:15. CrossRef Medline

Del Bigio MR (2010) Ependymal cells: biology and pathology. Acta Neuropathol 119:55–73. CrossRef Medline

Delling M, DeCaen PG, Doerner JF, Febvay S, Clapham DE (2013) Primary cilia are specialized calcium signalling organelles. Nature 504:311–314. CrossRef Medline

Field S, Riley KL, Grimes DT, Hilton H, Simon M, Powles-Glover N, Siggers P, Bogani D, Greenfield A, Norris DP (2011) Pkd1l1 establishes left-right asymmetry and physically interacts with Pkd2. Development 138:1131–1142. CrossRef Medline

Fuentealba LC, Obernier K, Alvarez-Buylla A (2012) Adult neural stem cells bridge their niche. Cell Stem Cell 10:698–708. CrossRef Medline

Garcia-Gonzalez MA, Outeda P, Zhou Q, Zhou F, Menezes LF, Qian F, Huso DL, Germino GG, Piontek KB, Watnick T (2010) Pkd1 and Pkd2 are required for normal placental development. PLoS One 5:e12821. CrossRef Medline

Guemez-Gamboa A, Coufal NG, Gleeson JG (2014) Primary cilia in the developing and mature brain. Neuron 82:511–521. CrossRef Medline

Guirao B, Meunier A, Mortaud S, Aguilar A, Corsi JM, Strehl L, Hirota Y, Desoeuvre A, Boutin C, Han YG, Mirzadeh Z, Cremer H, Montcouquiol M, Sawamoto K, Spassky N (2010) Coupling between hydrodynamic forces and planar cell polarity orients mammalian motile cilia. Nat Cell Biol 12:341–350. CrossRef Medline

Hanaoka K, Qian F, Boletta A, Bhunia AK, Piontek K, Tsiokas L, Sukhatme VP, Guggino WB, Germino GG (2000) Co-assembly of polycystin-1 and -2 produces unique cation-permeable currents. Nature 408:990–994. CrossRef Medline

Haycraft CJ, Zhang Q, Song B, Jackson WS, Detloff PJ, Serra R, Yoder BK (2007) Intraflagellar transport is essential for endochondral bone formation. Development 134:307–316. CrossRef Medline

Higginbotham H, Guo J, Yokota Y, Umberger NL, Su CY, Li J, Verma N, Hirt J, Ghukasyan V, Caspary T, Anton ES (2013) Arl13b-regulated cilia activities are essential for polarized radial glial scaffold formation. Nat Neurosci 16:1000–1007. CrossRef Medline

Hirota Y, Meunier A, Huang S, Shimozawa T, Yamada O, Kida YS, Inoue M, Ito T, Kato H, Sakaguchi M, Sunabori T, Nakaya MA, Nonaka S, Ogura T, Higuchi H, Okano H, Spassky N, Sawamoto K (2010) Planar polarity of multiciliated ependymal cells involves the anterior migration of basal bodies regulated by non-muscle myosin II. Development 137:3037–3046. CrossRef Medline

Iliescu A, Gravel M, Horth C, Kibar Z, Gros P (2011) Loss of membrane targeting of Vangl proteins causes neural tube defects. Biochemistry 50:795–804. CrossRef Medline

Jones C, Roper VC, Foucher I, Qian D, Banizs B, Petit C, Yoder BK, Chen P (2008) Ciliary proteins link basal body polarization to planar cell polarity regulation. Nat Genet 40:69–77. CrossRef Medline

Kamura K, Kobayashi D, Uehara Y, Koshida S, Iijima N, Kudo A, Yokoyama T, Takeda H (2011) Pkd1l1 complexes with Pkd2 on motile cilia and functions to establish the left-right axis. Development 138:1121–1129. CrossRef Medline

Kibar Z, Vogan KJ, Groulx N, Justice MJ, Underhill DA, Gros P (2001) Ltap, a mammalian homolog of *Drosophila Strabismus/Van Gogh*, is altered in the mouse neural tube mutant Loop-tail. Nat Genet 28:251–255. CrossRef Medline

Kim H, Xu H, Yao Q, Li W, Huang Q, Outeda P, Cebotaru V, Chiaravalli M, Boletta A, Piontek K, Germino GG, Weinman EJ, Watnick T, Qian F (2014) Ciliary membrane proteins traffic through the Golgi via a Rabep1/GGA1/Arl3-dependent mechanism. Nat Commun 5:5482. CrossRef Medline

Kotsis F, Boehlke C, Kuehn EW (2013) The ciliary flow sensor and polycystic kidney disease. Nephrol Dial Transplant 28:518–526. CrossRef Medline

Lee KL, Guevarra MD, Nguyen AM, Chua MC, Wang Y, Jacobs CR (2015) The primary cilium functions as a mechanical and calcium signaling nexus. Cilia 4:7. CrossRef Medline

Lee L (2013) Riding the wave of ependymal cilia: genetic susceptibility to hydrocephalus in primary ciliary dyskinesia. J Neurosci Res 91:1117–1132. CrossRef Medline

Luyten A, Su X, Gondela S, Chen Y, Rompani S, Takakura A, Zhou J (2010) Aberrant regulation of planar cell polarity in polycystic kidney disease. J Am Soc Nephrol 21:1521–1532. CrossRef Medline

Marszalek JR, Liu X, Roberts EA, Chui D, Marth JD, Williams DS, Goldstein LS (2000) Genetic evidence for selective transport of opsin and arrestin by kinesin-II in mammalian photoreceptors. Cell 102:175–187. CrossRef Medline

Merte J, Jensen D, Wright K, Sarsfield S, Wang Y, Schekman R, Ginty DD (2010) Sec24b selectively sorts Vangl2 to regulate planar cell polarity during neural tube closure. Nat Cell Biol 12:41–46; 1–8. CrossRef Medline

Mirzadeh Z, Merkle FT, Soriano-Navarro M, Garcia-Verdugo JM, Alvarez-Buylla A (2008) Neural stem cells confer unique pinwheel architecture to the ventricular surface in neurogenic regions of the adult brain. Cell Stem Cell 3:265–278. CrossRef Medline

Mirzadeh Z, Doetsch F, Sawamoto K, Wichterle H, Alvarez-Buylla A (2010a) The subventricular zone en-face: wholemount staining and ependymal flow. J Vis Exp 39:1938. CrossRef Medline

Mirzadeh Z, Han YG, Soriano-Navarro M, García-Verdugo JM, Alvarez-Buylla A (2010b) Cilia organize ependymal planar polarity. J Neurosci 30:2600–2610. CrossRef Medline

Mitchell B, Jacobs R, Li J, Chien S, Kintner C (2007) A positive feedback mechanism governs the polarity and motion of motile cilia. Nature 447:97–101. CrossRef Medline

Miyan JA, Nabiyouni M, Zendah M (2003) Development of the brain: a vital role for cerebrospinal fluid. Can J Physiol Pharmacol 81:317–328. CrossRef Medline

Montcouquiol M, Sans N, Huss D, Kach J, Dickman JD, Forge A, Rachel RA, Copeland NG, Jenkins NA, Bogani D, Murdoch J, Warchol ME, Wenthold RJ, Kelley MW (2006) Asymmetric localization of Vangl2 and Fz3 indicate novel mechanisms for planar cell polarity in mammals. J Neurosci 26:5265–5275. CrossRef Medline

Murdoch JN, Doudney K, Paternotte C, Copp AJ, Stanier P (2001) Severe neural tube defects in the loop-tail mouse result from mutation of Lpp1, a novel gene involved in floor plate specification. Hum Mol Genet 10:2593–2601. CrossRef Medline

Nauli SM, Alenghat FJ, Luo Y, Williams E, Vassilev P, Li X, Elia AE, Lu W, Brown EM, Quinn SJ, Ingber DE, Zhou J (2003) Polycystins 1 and 2 mediate mechanosensation in the primary cilium of kidney cells. Nat Genet 33:129–137. CrossRef Medline

Ohata S, Kinoshita S, Aoki R, Tanaka H, Wada H, Tsuruoka-Kinoshita S, Tsuboi T, Watabe S, Okamoto H (2009) Neuroepithelial cells require fucosylated glycans to guide the migration of vagus motor neuron progenitors in the developing zebrafish hindbrain. Development 136:1653–1663. CrossRef Medline

Ohata S, Aoki R, Kinoshita S, Yamaguchi M, Tsuruoka-Kinoshita S, Tanaka H, Wada H, Watabe S, Tsuboi T, Masai I, Okamoto H (2011) Dual roles of Notch in regulation of apically restricted mitosis and apicobasal polarity of neuroepithelial cells. Neuron 69:215–230. CrossRef Medline

Ohata S, Nakatani J, Herranz-Pérez V, Cheng J, Belinson H, Inubushi T, Snider WD, García-Verdugo JM, Wynshaw-Boris A, Alvarez-Buylla A (2014) Loss of dishevelleds disrupts planar polarity in ependymal motile cilia and results in hydrocephalus. Neuron 83:558–571. CrossRef Medline

Peng Y, Axelrod JD (2012) Asymmetric protein localization in planar cell polarity: mechanisms, puzzles, and challenges. Curr Top Dev Biol 101:33–53. CrossRef Medline

Qian F, Germino FJ, Cai Y, Zhang X, Somlo S, Germino GG (1997) PKD1 interacts with PKD2 through a probable coiled-coil domain. Nat Genet 16:179–183. CrossRef Medline

Sawamoto K, Wichterle H, Gonzalez-Perez O, Cholfin JA, Yamada M, Spassky N, Murcia NS, Garcia-Verdugo JM, Marin O, Rubenstein JL,

Tessier-Lavigne M, Okano H, Alvarez-Buylla A (2006) New neurons follow the flow of cerebrospinal fluid in the adult brain. Science 311:629–632. CrossRef Medline

Sharif-Naeini R, Folgering JH, Bichet D, Duprat F, Lauritzen I, Arhatte M, Jodar M, Dedman A, Chatelain FC, Schulte U, Retailleau K, Loufrani L, Patel A, Sachs F, Delmas P, Peters DJ, Honoré E (2009) Polycystin-1 and -2 dosage regulates pressure sensing. Cell 139:587–596. CrossRef Medline

Shillingford JM, Piontek KB, Germino GG, Weimbs T (2010) Rapamycin ameliorates PKD resulting from conditional inactivation of Pkd1. J Am Soc Nephrol 21:489–497. CrossRef Medline

Shimada Y, Yonemura S, Ohkura H, Strutt D, Uemura T (2006) Polarized transport of Frizzled along the planar microtubule arrays in *Drosophila* wing epithelium. Dev Cell 10:209–222. CrossRef Medline

Sipe CW, Lu X (2011) Kif3a regulates planar polarization of auditory hair cells through both ciliary and non-ciliary mechanisms. Development 138:3441–3449. CrossRef Medline

Spassky N, Merkle FT, Flames N, Tramontin AD, García-Verdugo JM, Alvarez-Buylla A (2005) Adult ependymal cells are postmitotic and are derived from radial glial cells during embryogenesis. J Neurosci 25:10–18. CrossRef Medline

Steigelman KA, Lelli A, Wu X, Gao J, Lin S, Piontek K, Wodarczyk C, Boletta A, Kim H, Qian F, Germino G, Géléoc GS, Holt JR, Zuo J (2011) Polycystin-1 is required for stereocilia structure but not for mechanotransduction in inner ear hair cells. J Neurosci 31:12241–12250. CrossRef Medline

Strong LC, Hollander WF (1949) Hereditary loop-tail in the house mouse: accompanied by imperforate vagina and with lethal craniorachischisis when homozygous. J Hered 40:329–334.

Su S, Phua SC, DeRose R, Chiba S, Narita K, Kalugin PN, Katada T, Kontani K, Takeda S, Inoue T (2013) Genetically encoded calcium indicator illuminates calcium dynamics in primary cilia. Nat Methods 10:1105–1107. CrossRef Medline

Tissir F, Qu Y, Montcouquiol M, Zhou L, Komatsu K, Shi D, Fujimori T, Labeau J, Tyteca D, Courtoy P, Poumay Y, Uemura T, Goffinet AM (2010) Lack of cadherins Celsr2 and Celsr3 impairs ependymal ciliogenesis, leading to fatal hydrocephalus. Nat Neurosci 13:700–707. CrossRef Medline

Tong CK, Han YG, Shah JK, Obernier K, Guinto CD, Alvarez-Buylla A (2014) Primary cilia are required in a unique subpopulation of neural progenitors. Proc Natl Acad Sci U S A 111:12438–12443. CrossRef Medline

Tronche F, Kellendonk C, Kretz O, Gass P, Anlag K, Orban PC, Bock R, Klein R, Schütz G (1999) Disruption of the glucocorticoid receptor gene in the nervous system results in reduced anxiety. Nat Genet 23:99–103. CrossRef Medline

Tsiokas L, Kim E, Arnould T, Sukhatme VP, Walz G (1997) Homo- and heterodimeric interactions between the gene products of PKD1 and PKD2. Proc Natl Acad Sci U S A 94:6965–6970. CrossRef Medline

Vladar EK, Bayly RD, Sangoram AM, Scott MP, Axelrod JD (2012) Microtubules enable the planar cell polarity of airway cilia. Curr Biol 22:2203–2212. CrossRef Medline

Wodarczyk C, Rowe I, Chiaravalli M, Pema M, Qian F, Boletta A (2009) A novel mouse model reveals that polycystin-1 deficiency in ependyma and choroid plexus results in dysfunctional cilia and hydrocephalus. PLoS One 4:e7137. CrossRef Medline

Ying G, Avasthi P, Irwin M, Gerstner CD, Frederick JM, Lucero MT, Baehr W (2014) Centrin 2 is required for mouse olfactory ciliary trafficking and development of ependymal cilia planar polarity. J Neurosci 34:6377–6388. CrossRef Medline

Yoshiba S, Shiratori H, Kuo IY, Kawasumi A, Shinohara K, Nonaka S, Asai Y, Sasaki G, Belo JA, Sasaki H, Nakai J, Dworniczak B, Ehrlich BE, Pennekamp P, Hamada H (2012) Cilia at the node of mouse embryos sense fluid flow for left-right determination via Pkd2. Science 338:226–231. CrossRef Medline

Zhou J (2009) Polycystins and primary cilia: primers for cell cycle progression. Annu Rev Physiol 71:83–113. CrossRef Medline

Zhuo L, Theis M, Alvarez-Maya I, Brenner M, Willecke K, Messing A (2001) hGFAP-cre transgenic mice for manipulation of glial and neuronal function *in vivo*. Genesis 31:85–94. CrossRef Medline